



Time-Critical Cooperative Path Following of Multiple Unmanned Aerial Vehicles over Time-Varying Networks

E. Xargay*

University of Illinois at Urbana-Champaign, Urbana, Illinois 61801

I. Kaminer†

Naval Postgraduate School, Monterey, California 93943

A. Pascoal‡

Instituto Superior Técnico, 1049 Lisbon, Portugal

N. Hovakimyan§

University of Illinois at Urbana-Champaign, Urbana, Illinois 61801

V. Dobrokhotov¶ and V. Cichella**

Naval Postgraduate School, Monterey, California 93943

A. P. Aguiar††

Instituto Superior Técnico, 1049 Lisbon, Portugal

and

R. Ghabcheloo‡‡

Tampere University of Technology, 33720 Tampere, Finland

DOI: 10.2514/1.56538

This paper addresses the problem of steering a fleet of unmanned aerial vehicles along desired three-dimensional paths while meeting stringent spatial and temporal constraints. A representative example is the challenging mission scenario where the unmanned aerial vehicles are tasked to cooperatively execute collision-free maneuvers and arrive at their final destinations at the same time. In the proposed framework, the unmanned aerial vehicles are assigned nominal spatial paths and speed profiles along those, and then the vehicles are requested to execute cooperative path following, rather than open loop trajectory tracking maneuvers. This strategy yields robust behavior against external disturbances by allowing the unmanned aerial vehicles to negotiate their speeds along the paths in response to information exchanged over the supporting communications network. The paper considers the case where the graph that captures the underlying time-varying communications topology is disconnected during some interval of time or even fails to be connected at all times. Conditions are given under which the cooperative path-following closed-loop system is stable. Flight test results of a coordinated road-search mission demonstrate the efficacy of the multi-vehicle cooperative control framework developed in the paper.

I. Introduction

UNMANNED aerial vehicles (UAVs) are becoming ubiquitous and have been playing an increasingly important role in military reconnaissance and strike operations, border-patrol missions, forest-fire detection, police surveillance, and recovery operations, to name

Received 7 October 2011; revision received 25 May 2012; accepted for publication 31 May 2012; published online 7 February 2013. Copyright © 2012 by E. Xargay, I. Kaminer, A. Pascoal, N. Hovakimyan, V. Dobrokhotov, V. Cichella, A. P. Aguiar, and R. Ghabcheloo. Published by the American Institute of Aeronautics and Astronautics, Inc., with permission. Copies of this paper may be made for personal or internal use, on condition that the copier pay the \$10.00 per-copy fee to the Copyright Clearance Center, Inc., 222 Rosewood Drive, Danvers, MA 01923; include the code 1533-3884/13 and \$10.00 in correspondence with the CCC.

*Ph.D. Candidate, Department of Aerospace Engineering; xargay@illinois.edu. Student Member AIAA.

†Professor, Department of Mechanical and Astronautical Engineering; kaminer@nps.edu. Member AIAA.

‡Associate Professor, Laboratory of Robotics and Systems in Engineering and Science; antonio@isr.ist.utl.pt. Member AIAA.

§Professor, Department of Mechanical Science and Engineering; nhovakim@illinois.edu. Associate Fellow AIAA.

¶Associate Research Professor, Department of Mechanical and Astronautical Engineering; vldobr@nps.edu. Senior Member AIAA.

**Research Associate, Department of Mechanical and Astronautical Engineering; venanzio.cichella@gmail.com. Student Member AIAA.

††Assistant Professor, Laboratory of Robotics and Systems in Engineering and Science; pedro@isr.ist.utl.pt. Member AIAA.

‡‡Senior Researcher, Department of Intelligent Hydraulics and Automation; reza.ghabcheloo@tut.fi. Member AIAA.

but a few. In simple applications, a single autonomous vehicle can be managed by a crew using a ground station provided by the vehicle manufacturer. The execution of more challenging missions, however, requires the use of multiple vehicles working in cooperation to achieve a common objective. Representative examples of cooperative mission scenarios are sequential auto-landing and coordinated ground-target suppression for multiple UAVs. The first refers to the situation where a fleet of UAVs must break up and arrive at the assigned glideslope point, separated by prespecified safeguarding time intervals. In the case of ground-target suppression, a formation of UAVs must also break up and execute a coordinated maneuver to arrive at predefined positions over the target at the same time.

In both cases, only relative (rather than absolute) temporal constraints are given a priori, a critical point that needs to be emphasized. Furthermore, the vehicles must execute maneuvers in close proximity to each other. In addition, as pointed out in [1,2], the flow of information among vehicles may be severely restricted, either for security reasons or because of tight bandwidth limitations. As a consequence, no vehicle might be able to communicate with the entire formation, and the amount of information that can be exchanged might be limited. Moreover, the topology of the intervehicle communications network supporting the cooperative mission may change over time. Under these circumstances, it is important to develop cooperative motion-control strategies that can yield robust performance in the presence of time-varying communications networks arising from temporary loss of communications links and switching communications topologies.

Motivated by these and similar problems, there has been increasing interest over the past few years in the study of multi-agent system

networks with applications to engineering and science problems. The range of topics addressed include parallel computing [3], synchronization of oscillators [4], study of collective behavior and flocking [5], multisystem consensus mechanisms [6], multivehicle system formations [7–10], coordinated motion control [11–13], cooperative path and trajectory planning [14–18], asynchronous protocols [19], dynamic graphs [20], stochastic graphs [20–22], and graph-related theory [2,23]. Especially relevant are the applications of the theory developed in the area of multivehicle formation control: spacecraft formation flying [24], UAV control [25,26], coordinated control of land robots [11], and control of multiple autonomous underwater vehicles and surface vessels [27–36]. In spite of significant progress in the field, much work remains to be done to develop strategies capable of yielding robust performance of a fleet of vehicles in the presence of complex vehicle dynamics, communications constraints, and partial vehicle failures.

It is against this backdrop of ideas that this paper addresses the problem of steering a fleet of UAVs along desired paths while meeting stringent spatial and temporal constraints. The cooperative missions considered here require that the UAVs follow collision-free paths and that all vehicles arrive at their final destinations at the same time (time-critical operations). In the adopted setup, the vehicles are assigned desired nominal paths and speed profiles along them. The paths are then appropriately parameterized, and the vehicles are requested to execute cooperative path following, rather than open-loop trajectory-tracking maneuvers. This strategy yields robust performance in the face of external disturbances by allowing the vehicles to negotiate their speeds along the paths in response to information exchanged over the supporting communications network. Moreover, as proven in [37], the path-following approach is not subject to the fundamental performance limitations of trajectory tracking in the presence of unstable zero dynamics. The paper builds upon previous work by the authors on time-critical cooperative path following and extends it to a very general framework that allows for the consideration of complex vehicle dynamics and time-varying communications topologies in a rigorous mathematical setting. The reader is referred to [38–43] and the references therein for an introduction to the subject and a general perspective of the circle of ideas that are at the root of the present work. From a technical point of view, the present paper departs substantially from previous published work in two key aspects.

1) It puts forward a new algorithm for path following in three-dimensional (3-D) space that uses the special orthogonal group $\text{SO}(3)$ in the formulation of the attitude-control problem. This formulation avoids the geometric singularities and complexities that appear when dealing with local parameterizations of the vehicle's attitude and thus leads to a singularity-free path-following control law.

2) It offers a new proof of convergence of the relevant variables involved in cooperative path following that significantly simplifies the one summarized in [40] and extends it to the case where the speed profiles of the different vehicles along their paths are arbitrary but meet desired geometrical constraints. In the setup adopted, the communications graph that captures the underlying communications network topology is allowed to be disconnected during some interval of time or may even fail to be connected at all times. It is shown that, if the connectivity of the communications graph satisfies a certain persistency of excitation (PE)-like condition, then the UAVs “reach consensus” in the sense that a conveniently defined cooperation error converges to a neighborhood of the origin. The paper also derives lower bounds on the convergence rate of the collective dynamics as a function of the level of connectivity of the dynamic communications graph.

To demonstrate the efficacy of the developed algorithms, the paper also presents flight-test results of a coordinated road-search mission that exploits the multi-UAV cooperative control framework developed. These experimental results build on the ones reported in [44] by analyzing in greater detail the performance of the road-search mission.

This paper is organized as follows. Section II formulates the time-critical cooperative path-following problem, describes the kinemat-

ics of the systems of interest, and introduces a set of assumptions and limitations on the supporting communications network. Section III presents a path-following control algorithm for UAVs in 3-D space. Section IV derives a strategy for time-critical cooperative path following of multiple UAVs in the presence of time-varying communications networks that relies on the adjustment of the desired speed profile of each vehicle. Section V addresses the stability and convergence properties of the combined coordination and path-following systems. Section VI presents actual flight-test results performed in Camp Roberts, CA. Finally, Sec. VII summarizes the key results and contains the main conclusions.

The following notation is used throughout the paper. $\{v\}_F$ is used to denote the vector v resolved in frame F ; $\{\mathbf{e}\}_F$ represents the versor \mathbf{e} resolved in frame F ; $\omega_{F1/F2}$ denotes the angular velocity of frame $F1$ with respect to frame $F2$; the rotation matrix from frame $F1$ to frame $F2$ is represented by R_{F1}^{F2} ; and $\dot{v}|_F$ indicates that the time-derivative of vector v is taken in frame F . Moreover, unless otherwise noted, $\|\cdot\|$ is used for both the 2-norm of a vector and the induced 2-norm of a matrix. Finally, $\text{SO}(3)$ denotes the special orthogonal group in Euclidean 3-space, while $\mathfrak{so}(3)$ represents the set of 3×3 skew-symmetric matrices over \mathbb{R} .

II. Time-Critical Cooperative Path Following: Problem Formulation

This section provides a rigorous formulation of the problem of time-critical cooperative path-following control for multiple UAVs in 3-D space, in which a fleet of UAVs is tasked to converge to and follow a set of desired feasible paths so as to meet spatial and temporal constraints. The section also introduces a set of assumptions and limitations on the supporting communications network.

The problem of cooperative trajectory generation is not addressed in this paper. In fact, it is assumed that a set of desired 3-D time trajectories $p_{d,i}(t_d): \mathbb{R} \rightarrow \mathbb{R}^3$, conveniently parameterized by a single time variable $t_d \in [0, t_d^*]$, is known for all of the n UAVs involved in a cooperative mission. The variable t_d represents a desired mission time (distinct from the actual mission time that evolves as the mission unfolds), with t_d^* being the desired mission duration. For a given t_d , $p_{d,i}(t_d)$ defines the desired position of the i th UAV t_d seconds after the initiation of the cooperative mission. These time trajectories can be reparameterized in terms of path length to obtain spatial paths $p_{d,i}(\tau_{\ell,i}): \mathbb{R} \rightarrow \mathbb{R}^3$ (with no temporal specifications) and the corresponding desired speed profiles $v_{d,i}(t_d): \mathbb{R} \rightarrow \mathbb{R}$. For convenience, each spatial path is parameterized by its path length $\tau_{\ell,i} \in [0, \ell_{fi}]$, where ℓ_{fi} denotes the total length of the i th path, whereas the desired speed profiles are parameterized by the desired mission time t_d . It is assumed that both the paths and the speed profiles satisfy collision-avoidance constraints as well as appropriate boundary and feasibility conditions, such as those imposed by the physical limitations of the UAVs. In particular, in the context of this paper, it is assumed that the paths are spatially deconflicted with spatial clearance $E > 0$. (The results in the present paper can be easily extended to time-deconflicted paths; one only needs to replace the condition in Theorem 1 that relates the spatial clearance E to the path-following and coordination error bounds; see Remark 6.) It is further assumed that the rate and speed commands required to follow the paths and achieve time coordination do not result in the UAVs operating outside their normal flight envelope and do not lead to internal saturation of the onboard autopilots. The problem of generation of feasible collision-free trajectories for multiple cooperative autonomous vehicles is described in detail in [44].

A. Path Following for a Single Unmanned Aerial Vehicle

Pioneering work in the area of path following can be found in [45], where an elegant solution to the problem was presented for a wheeled robot at the kinematic level. In the setup adopted, the kinematic model of the vehicle was derived with respect to a Frenet–Serret frame moving along the path, while playing the role of a virtual target vehicle to be tracked by the real vehicle. The origin of the Frenet–Serret was placed at the point on the path closest to the real vehicle.

This work spurred a great deal of activity in the literature addressing the path-following control problem. Of particular interest is the work reported in [46], in which the authors reformulated the setup used in [45] and derived a feedback control law that steers the dynamic model of a wheeled robot along a desired path and overcomes stringent initial condition constraints present in [45]. The key to the algorithm in [46] is to explicitly control the rate of progression of the virtual target along the path. This effectively creates an extra degree of freedom that can be exploited to avoid singularities that occur when the distance to the path is not well defined.

The solution to the path-following problem described in the present paper extends to the 3-D case the algorithm presented in [46], and relies on the insight that a UAV can follow a given path using only its attitude, thus leaving its speed as an extra degree of freedom to be used at the coordination level. The key idea of the algorithm is to use the vehicle's attitude-control effectors to follow a virtual target vehicle running along the path. To this effect, following the approach developed in [46], this section introduces a frame attached to this virtual target and defines a generalized error vector between this moving coordinate system and a frame attached to the actual vehicle. With this setup, the path-following control problem is reduced to that of driving this generalized error vector to zero by using only the UAV's attitude-control effectors, while following an arbitrary feasible speed profile. Next, the dynamics of the kinematic errors between the i th vehicle and its virtual target are characterized.

Figure 1 captures the geometry of the problem at hand. Let $p_d(\cdot)$ be the desired path assigned to one of the UAVs, and let ℓ_f be its total length. Let \mathcal{I} denote an inertial reference frame $\{\mathbf{e}_{I1}, \mathbf{e}_{I2}, \mathbf{e}_{I3}\}$, and let $p_I(t)$ be the position of the center of mass Q of the UAV in this inertial frame. Further, let P be an arbitrary point on the desired path that plays the role of the virtual target, and let $p_d(\ell)$ denote its position in the inertial frame. Here, $\ell \in [0, \ell_f]$ is a free-length variable that defines the position of the virtual target vehicle along the path. In the setup adopted, the total rate of progression of the virtual target along the path is an extra design parameter. This approach is in striking contrast with the strategy used in the path-following algorithm introduced in [45], where P is defined as the point on the path that is closest to the vehicle. Endowing point P with an extra degree of freedom is the key to the path-following algorithm presented in [46] and its extension to the 3-D case described in this paper.

For our purposes, it is convenient to define a parallel transport frame \mathcal{F} attached to point P on the path and characterized by the orthonormal vectors $\{\mathbf{t}(\ell), \mathbf{n}_1(\ell), \mathbf{n}_2(\ell)\}$, which satisfy the following frame equations [47,48]:

$$\begin{bmatrix} \frac{d\mathbf{t}}{d\ell}(\ell) \\ \frac{d\mathbf{n}_1}{d\ell}(\ell) \\ \frac{d\mathbf{n}_2}{d\ell}(\ell) \end{bmatrix} = \begin{bmatrix} 0 & k_1(\ell) & k_2(\ell) \\ -k_1(\ell) & 0 & 0 \\ -k_2(\ell) & 0 & 0 \end{bmatrix} \begin{bmatrix} \mathbf{t}(\ell) \\ \mathbf{n}_1(\ell) \\ \mathbf{n}_2(\ell) \end{bmatrix}$$

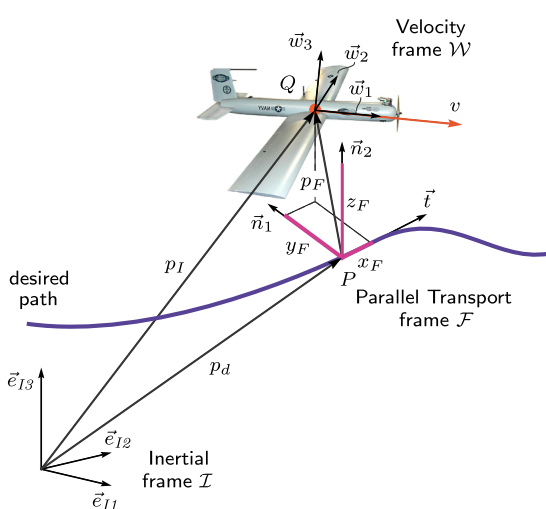


Fig. 1 Following a virtual target vehicle; problem geometry.

where $k_1(\ell)$ and $k_2(\ell)$ are related to the polar coordinates of curvature $\kappa(\ell)$ and torsion $\tau(\ell)$ as $\kappa(\ell) = (k_1^2(\ell) + k_2^2(\ell))^{\frac{1}{2}}$ and $\tau(\ell) = -\frac{d}{d\ell}(\tan^{-1}(k_2(\ell)/k_1(\ell)))$. The vectors $\{\mathbf{t}, \mathbf{n}_1, \mathbf{n}_2\}$ define an orthonormal basis for \mathcal{F} , in which the unit vector $\mathbf{t}(\ell)$ defines the tangent direction to the path at the point determined by ℓ , while $\mathbf{n}_1(\ell)$ and $\mathbf{n}_2(\ell)$ define the normal plane perpendicular to $\mathbf{t}(\ell)$. Unlike the Frenet-Serret frame, this moving frame is well defined when the path has a vanishing second derivative. This orthonormal basis can be used to construct the rotation matrix $R_F^I(\ell) = [\{\mathbf{t}(\ell)\}_I; \{\mathbf{n}_1(\ell)\}_I; \{\mathbf{n}_2(\ell)\}_I]$ from \mathcal{F} to \mathcal{I} . Furthermore, the angular velocity of \mathcal{F} with respect to \mathcal{I} , resolved in \mathcal{F} , can be easily expressed in terms of the parameters $k_1(\ell)$ and $k_2(\ell)$ as

$$\{\omega_{F/I}\}_F = [0, -k_2(\ell)\dot{\ell}, k_1(\ell)\dot{\ell}]^T$$

Let $p_F(t)$ be the position of the vehicle's center of mass Q in the parallel transport frame, and let $x_F(t)$, $y_F(t)$, and $z_F(t)$ be the components of vector $p_F(t)$ with respect to the basis $\{\mathbf{t}, \mathbf{n}_1, \mathbf{n}_2\}$, that is,

$$\{p_F\}_F = [x_F, y_F, z_F]^T$$

Finally, let \mathcal{W} denote a vehicle-carried velocity frame $\{\mathbf{w}_1, \mathbf{w}_2, \mathbf{w}_3\}$ with its origin at the UAV center of mass and its x axis aligned with the velocity vector of the UAV. The z axis is chosen to lie in the plane of symmetry of the UAV, and the y axis is determined by completing the right-hand system. In this paper, $q(t)$ and $r(t)$ are the y -axis and z -axis components, respectively, of the vehicle's rotational velocity resolved in the \mathcal{W} frame. With a slight abuse of notation, $q(t)$ and $r(t)$ will be referred to as pitch rate and yaw rate, respectively, in the \mathcal{W} frame.

Next, the previous notation is used to characterize the kinematic error dynamics of the UAV with respect to the virtual target. The position-error dynamics are derived first. For this purpose, note that

$$p_I = p_d(\ell) + p_F$$

from which it follows that

$$\dot{p}_I|_I = \dot{\ell}\mathbf{t} + \omega_{F/I} \times p_F + \dot{p}_F|_F$$

where $\cdot|_I$ and $\cdot|_F$ are used to indicate that the derivatives are taken in the inertial and parallel transport frames, respectively. Because

$$\dot{p}_F|_I = v\mathbf{w}_1$$

where $v(t)$ denotes the magnitude of the UAV's ground velocity vector, the path-following kinematic position-error dynamics of the UAV with respect to the virtual target can be written as

$$\dot{p}_F|_F = -\dot{\ell}\mathbf{t} - \omega_{F/I} \times p_F + v\mathbf{w}_1 \quad (1)$$

To derive the attitude-error dynamics of the UAV with respect to its virtual target, an auxiliary frame \mathcal{D} $\{\mathbf{b}_{1D}, \mathbf{b}_{2D}, \mathbf{b}_{3D}\}$ is first introduced. This frame will be used to shape the approach attitude to the path as a function of the "cross-track" error components y_F and z_F . Frame \mathcal{D} has its origin at the UAV center of mass, and vectors $\mathbf{b}_{1D}(t)$, $\mathbf{b}_{2D}(t)$, and $\mathbf{b}_{3D}(t)$ are defined as

$$\begin{aligned} \mathbf{b}_{1D} &\triangleq \frac{d\mathbf{t} - y_F\mathbf{n}_1 - z_F\mathbf{n}_2}{(d^2 + y_F^2 + z_F^2)^{\frac{1}{2}}}, & \mathbf{b}_{2D} &\triangleq \frac{y_F\mathbf{t} + d\mathbf{n}_1}{(d^2 + y_F^2)^{\frac{1}{2}}}, \\ \mathbf{b}_{3D} &\triangleq \mathbf{b}_{1D} \times \mathbf{b}_{2D} \end{aligned} \quad (2)$$

with d being a (positive) constant characteristic distance. The basis vector $\mathbf{b}_{1D}(t)$ defines the desired direction of the UAV's velocity vector. Clearly, when the vehicle is far from the desired path, vector $\mathbf{b}_{1D}(t)$ becomes perpendicular to $\mathbf{t}(\ell)$. As the vehicle comes closer to the path and the cross-track error becomes smaller, then $\mathbf{b}_{1D}(t)$ tends to $\mathbf{t}(\ell)$.

Next, let $\tilde{R}(t) \in \text{SO}(3)$ be the rotation matrix from \mathcal{W} to \mathcal{D} , that is,

$$\tilde{R} \triangleq R_W^D = R_F^D R_W^F = (R_D^F)^T R_W^F$$

and define the real-valued error function on $\text{SO}(3)$

$$\Psi(\tilde{R}) \triangleq \frac{1}{2} \text{tr}[(\mathbb{I}_3 - \Pi_R^T \Pi_R)(\mathbb{I}_3 - \tilde{R})] \quad (3)$$

where Π_R is defined as $\Pi_R \triangleq \begin{bmatrix} 0 & 1 & 0 \\ 0 & 0 & 1 \end{bmatrix}$. The function $\Psi(\tilde{R})$ in

Eq. (3) can be expressed in terms of the entries of $\tilde{R}(t)$ as $\Psi(\tilde{R}) = (1/2)(1 - \tilde{R}_{11})$, where $\tilde{R}_{11}(t)$ denotes the (1,1) entry of $\tilde{R}(t)$. Therefore, $\Psi(\tilde{R})$ is a positive-definite function about $\tilde{R}_{11} = 1$. Note that $\tilde{R}_{11} = 1$ corresponds to the situation where the velocity vector of the UAV is aligned with the basis vector $\mathbf{b}_{1D}(t)$, which defines the desired attitude.

The attitude kinematics equation

$$\dot{\tilde{R}} = \dot{R}_W^D = R_W^D (\{\omega_{W/D}\}_W)^\wedge = \tilde{R} (\{\omega_{W/D}\}_W)^\wedge$$

where $(\cdot)^\wedge: \mathbb{R}^3 \rightarrow \mathfrak{so}(3)$ denotes the hat map (see Appendix A), can be used to derive the time derivative of $\Psi(\tilde{R})$, given by

$$\dot{\Psi}(\tilde{R}) = -\frac{1}{2} \text{tr}[(\mathbb{I}_3 - \Pi_R^T \Pi_R)\tilde{R} (\{\omega_{W/D}\}_W)^\wedge]$$

Equation (A1) of the hat map (see Appendix A) leads to

$$\dot{\Psi}(\tilde{R}) = \frac{1}{2} ((\mathbb{I}_3 - \Pi_R^T \Pi_R)\tilde{R} - \tilde{R}^T (\mathbb{I}_3 - \Pi_R^T \Pi_R))^\vee T \{\omega_{W/D}\}_W$$

where $(\cdot)^\vee: \mathfrak{so}(3) \rightarrow \mathbb{R}^3$ denotes the vee map, which is defined as the inverse of the hat map. Moreover, because the first component of the vector $((\mathbb{I}_3 - \Pi_R^T \Pi_R)\tilde{R} - \tilde{R}^T (\mathbb{I}_3 - \Pi_R^T \Pi_R))^\vee$ is equal to zero, one can also write

$$\dot{\Psi}(\tilde{R}) = \left(\frac{1}{2} \Pi_R ((\mathbb{I}_3 - \Pi_R^T \Pi_R)\tilde{R} - \tilde{R}^T (\mathbb{I}_3 - \Pi_R^T \Pi_R))^\vee \right)^T \Pi_R \{\omega_{W/D}\}_W \quad (4)$$

Next, define the attitude error $e_{\tilde{R}}(t)$ as

$$e_{\tilde{R}} \triangleq \frac{1}{2} \Pi_R ((\mathbb{I}_3 - \Pi_R^T \Pi_R)\tilde{R} - \tilde{R}^T (\mathbb{I}_3 - \Pi_R^T \Pi_R))^\vee$$

which allows Eq. (4) to be rewritten in the more compact form

$$\dot{\Psi}(\tilde{R}) = e_{\tilde{R}} \cdot (\Pi_R \{\omega_{W/D}\}_W)$$

Note that the attitude error $e_{\tilde{R}}(t)$ can also be expressed in terms of the entries of $\tilde{R}(t)$ as $e_{\tilde{R}} = (1/2)[\tilde{R}_{13}, -\tilde{R}_{12}]^T$ and, therefore, within the region where $\Psi(\tilde{R}) < 1$, one has that, if $\|e_{\tilde{R}}\| = 0$, then $\tilde{R}_{11} = 1$. Finally, noting that $\{\omega_{W/F}\}_W$ can be expressed as

$$\begin{aligned} \{\omega_{W/D}\}_W &= \{\omega_{W/I}\}_W + \{\omega_{I/F}\}_W + \{\omega_{D/F}\}_W \\ &= \{\omega_{W/I}\}_W - \tilde{R}^T (R_F^D \{\omega_{F/I}\}_F + \{\omega_{D/F}\}_D) \end{aligned}$$

one obtains

$$\dot{\Psi}(\tilde{R}) = e_{\tilde{R}} \cdot \left(\begin{bmatrix} q \\ r \end{bmatrix} - \Pi_R \tilde{R}^T (R_F^D \{\omega_{F/I}\}_F + \{\omega_{D/F}\}_D) \right) \quad (5)$$

This equation describes the path-following kinematic attitude-error dynamics of frame \mathcal{W} with respect to frame \mathcal{D} . The path-following kinematic-error dynamics \mathcal{G}_e can now be obtained by combining Eqs. (1) and (5), yielding

$$\dot{p}_F]_F = -\dot{\ell} \mathbf{t} - \omega_{F/I} \times p_F + v \mathbf{w}_1,$$

$$\dot{\Psi}(\tilde{R}) = e_{\tilde{R}} \cdot \left(\begin{bmatrix} q \\ r \end{bmatrix} - \Pi_R \tilde{R}^T (R_F^D \{\omega_{F/I}\}_F + \{\omega_{D/F}\}_D) \right) \quad (6)$$

In the kinematic-error model [Eq. (6)], $q(t)$ and $r(t)$ play the role of control inputs, while the rate of progression $\dot{\ell}(t)$ of point P along the path becomes an extra variable that can be manipulated at will. At this point, the path-following generalized error vector $x_{pf}(t)$ can be formally defined as

$$x_{pf} \triangleq [p_F^T, e_{\tilde{R}}^T]^T$$

Notice that, within the region where $\Psi(\tilde{R}) < 1$, if $x_{pf} = 0$, then both the path-following position error and the path-following attitude error are equal to zero, that is $p_F = 0$ and $R_{11} = 1$.

Using the previous formulation, and given a spatially defined feasible path $p_d(\cdot)$, the problem of path following for a single vehicle can now be defined.

Definition 1 (path-following problem): For a given UAV (equipped with an autopilot), design feedback control laws for pitch rate $q(t)$, yaw rate $r(t)$, and rate of progression $\dot{\ell}(t)$ of the virtual target along the path such that all closed-loop signals are bounded and the path-following generalized error vector $x_{pf}(t)$ converges to a neighborhood of the origin with a guaranteed rate of convergence, regardless of what the temporal speed assignment of the mission is (as long as it is physically feasible).

Stated in simple terms, the previous problem amounts to designing feedback laws so that a UAV converges to and remains inside a tube centered on the desired path curve assigned to this UAV, for an arbitrary speed profile (subject to feasibility constraints).

B. Time-Critical Coordination and Network Model

To enforce the temporal constraints that must be met in real time to coordinate the entire fleet of vehicles, the speed profile of each vehicle is adjusted based on coordination information exchanged among the UAVs over a time-varying communications network. To this effect, an appropriate coordination variable needs to be defined for each vehicle that captures the objective of the cooperative mission, in our case, simultaneous arrival of all the UAVs at their final destinations.

For this purpose, let $\ell'_{d,i}(t_d)$ be defined as the desired normalized curvilinear abscissa of the i th UAV along its corresponding path at the desired mission time t_d , which is given by

$$\ell'_{d,i}(t_d) \triangleq \frac{1}{\ell_{fi}} \int_0^{t_d} v_{d,i}(\tau) d\tau$$

with ℓ_{fi} and $v_{d,i}(\cdot)$ being, respectively, the length of the path and the desired speed profile corresponding to the i th UAV. The trajectory-generation algorithm ensures that the desired speed profiles $v_{d,i}(\cdot)$ satisfy feasibility conditions, which implies that the following bounds hold for all vehicles:

$$0 < v_{\min} \leq v_{d,i \min} \leq v_{d,i \max} \leq v_{\max}, \quad i = 1, \dots, n \quad (7)$$

where v_{\min} and v_{\max} denote, respectively, the minimum and maximum operating speeds of the UAVs involved in the cooperative mission, while $v_{d,i \min}$ and $v_{d,i \max}$ denote lower and upper bounds on the desired speed profile for the i th UAV. From the definition of $\ell'_{d,i}(t_d)$ and the bounds in Eq. (7), it follows that $\ell'_{d,i}(t_d)$ is a strictly increasing continuous function of t_d mapping $[0, t_d^*]$ onto $[0, 1]$, and satisfying $\ell'_{d,i}(0) = 0$ and $\ell'_{d,i}(t_d^*) = 1$. Define also $\eta_i: [0, 1] \rightarrow [0, t_d^*]$ to be the inverse function of $\ell'_{d,i}(t_d)$, $t_d \in [0, t_d^*]$. Clearly, $\eta_i(\cdot)$ is also a strictly increasing continuous function of its argument. Then, letting $\ell'_i(t)$ be the normalized curvilinear abscissa at time t of the i th virtual target vehicle running along its path, defined as

$$\ell'_i(t) \triangleq \frac{\ell_i(t)}{\ell_{fi}}$$

where $\ell_i(t) \in [0, \ell_{fi}]$ was introduced in the previous section, define the time variables

$$\xi_i(t) \triangleq \eta_i(\ell'_i(t)), \quad i = 1, \dots, n$$

From this definition, it follows that $\xi_i(t) \in [0, t_d^*]$, and therefore this variable can be seen as a virtual time that characterizes the status of the mission for the i th UAV at time t in terms of the desired mission time t_d .

Note that, for any two vehicles i and j , if $\xi_i(t) = \xi_j(t) = t_d'$ at a given time t , then $\ell'_i(t) = \ell'_{d,i}(t_d')$ and $\ell'_j(t) = \ell'_{d,j}(t_d')$, which implies that at time t the target vehicles corresponding to UAVs i and j have the desired relative position along the path at the desired mission time t_d' . Clearly, if $\xi_i(t) = \xi_j(t)$ for all $t \geq 0$, then the i th and j th virtual target vehicles maintain desired relative position along the path at all times and, in particular, these two target vehicles arrive at their final destinations at the same time, which does not necessarily correspond to the desired mission duration t_d^* . Also, in the case of collision avoidance in time (see [44]), if $\xi_i(t) = \xi_j(t)$ for all $t \geq 0$, then the solution to the trajectory-generation problem ensures that the virtual targets i and j do not collide. Moreover, if the i th virtual target travels at the desired speed for all time in the interval $[0, t]$, that is $\dot{\ell}_i(\tau) = v_{d,i}(\tau)$ for all $\tau \in [0, t]$, then one has that $\ell_i(\tau) = \ell'_{d,i}(\tau)$ for all $\tau \in [0, t]$, which implies that $\xi_i(\tau) = \tau$ (or, equivalently, that $\dot{\xi}_i(\tau) = 1$) for all $\tau \in [0, t]$. This set of properties makes the variables $\xi_i(t)$ an appropriate metric for vehicle coordination, and therefore they will be referred to as coordination states. Notice that the use of these specific coordination variables is motivated by the work in [41].

To meet the desired temporal assignments of the cooperative mission, coordination information is to be exchanged among the UAVs over the supporting communications network. Next, tools and facts from algebraic graph theory are used to model the information exchange over the time-varying network as well as the constraints imposed by the communications topology (see for example [9,49] and references therein). The reader is also referred to [50] for key concepts and details on algebraic graph theory.

First, to account for the communications constraints imposed by this intervehicle network, it is assumed that the i th UAV can only exchange information with a neighboring set of vehicles, denoted here by \mathcal{N}_i . It is also assumed that the communications between two UAVs are bidirectional and that the information is transmitted continuously with no delays. Moreover, because the flow of information among vehicles may be severely restricted, either for security reasons or because of tight bandwidth limitations, each vehicle is only allowed to exchange its coordination state $\xi_i(t)$ with its neighbors. Finally, it is assumed that the connectivity of the communications graph $\Gamma(t)$ that captures the underlying bidirectional communications network topology of the fleet at time t satisfies the PE-like condition

$$\frac{1}{n} \frac{1}{T} \int_t^{t+T} QL(\tau)Q^T d\tau \geq \mu \mathbb{I}_{n-1}, \quad \text{for all } t \geq 0 \quad (8)$$

where $L(t) \in \mathbb{R}^{n \times n}$ is the Laplacian of the graph $\Gamma(t)$, and Q is an $(n-1) \times n$ matrix such that $Q\mathbf{1}_n = 0$ and $QQ^T = \mathbb{I}_{n-1}$, with $\mathbf{1}_n$ being the vector in \mathbb{R}^n whose components are all 1. The parameters $T, \mu > 0$ characterize the quality of service (QoS) of the communications network, which, in the context of this paper, represents a measure of the level of connectivity of the communications graph. Note that the PE-like condition of Eq. (8) requires only the communications graph $\Gamma(t)$ to be connected in an integral sense, not pointwise in time. In fact, the graph may be disconnected during some interval of time or may even fail to be connected for the entire duration of the mission. Similar type of conditions can be found, for example, in [6,51].

Using the previous formulation, one can now define the problem of time-critical cooperative path following for a fleet of n UAVs.

Definition 2 (time-critical cooperative path-following problem): Given a fleet of n vehicles supported by an intervehicle communications network and a set of desired 3-D time trajectories $p_{d,i}(t_d)$, design feedback control laws for pitch rate $q(t)$, yaw rate $r(t)$, and speed $v(t)$ such that 1) all closed-loop signals are bounded; 2) for each vehicle $i, i \in \{1, \dots, n\}$, the path-following generalized error vector $x_{pf,i}(t)$ converges to a neighborhood of the origin; and 3) for each pair of vehicles i and $j, i, j \in \{1, \dots, n\}$, the coordination error $|\xi_i(t) - \xi_j(t)|$ converges to a neighborhood of the origin, guaranteeing (quasi-)simultaneous time of arrival and ensuring collision-free maneuvers.

C. Unmanned Aerial Vehicle with Autopilot

At this point, it is important to stress that this paper addresses the design of control algorithms for path following and time coordination yielding robust performance of a fleet of UAVs executing various time-critical cooperative missions. These control algorithms are to be seen as guidance outer-loop controllers that provide reference commands to inner-loop autopilots stabilizing the UAV dynamics and providing angular-rate as well as speed-tracking capabilities. This inner/outer-loop approach simplifies the design process and affords the designer a systematic approach to seamlessly tailor the algorithms for a very general class of UAVs that come equipped with inner-loop commercial autopilots. The design of inner-loop onboard autopilots that are capable of tracking reference commands generated by outer-loop controllers and providing uniform performance across the flight envelope is, however, beyond the scope of the work presented here. This section presents a set of assumptions on the inner closed-loop performance of the UAVs with their autopilots, which will be useful to analyze the convergence properties of the path-following and coordination control laws developed later in the paper.

To this effect, and for the purpose of this paper, it is assumed that each UAV is equipped with an onboard autopilot designed to stabilize the UAV and to provide angular-rate as well as speed-tracking capabilities. In particular, the assumption is made that the onboard autopilots ensure that each UAV is able to track bounded pitch-rate and yaw-rate commands, denoted here by $q_c(t)$ and $r_c(t)$, with guaranteed performance bounds γ_q and γ_r . Stated mathematically,

$$|q_c(t) - q(t)| \leq \gamma_q, \quad \forall t \geq 0 \quad (9a)$$

$$|r_c(t) - r(t)| \leq \gamma_r, \quad \forall t \geq 0 \quad (9b)$$

Similarly, it is assumed that, if the speed commands $v_c(t)$ satisfy the bounds

$$v_{\min} \leq v_c(\tau) \leq v_{\max}, \quad \forall \tau \in [0, t] \quad (10)$$

then the autopilots ensure that each UAV tracks its corresponding speed command with guaranteed performance bound γ_v :

$$|v_c(\tau) - v(\tau)| \leq \gamma_v, \quad \forall \tau \in [0, t] \quad (11)$$

The bounds γ_q , γ_r , and γ_v thus characterize the level of tracking performance that the inner-loop autopilot is able to provide. It is important to note that, in this setup, it is the autopilot that determines the bank angle required to track the angular-rate commands $q_c(t)$ and $r_c(t)$. Therefore, it is justified to assume that the UAV roll dynamics (roll rate and bank angle) are bounded for bounded angular-rate commands corresponding to the set of feasible paths considered.

Remark 1: The bounds in Eqs. (9) and (11) will be used later in the paper to set constraints on the inner-loop tracking-performance requirements that guarantee stability of the complete cooperative control architecture. As it will become clear from the algorithms for path following and time coordination proposed later, a proper choice of the boundary (initial) conditions for the trajectory-generation problem may be required to ensure that these bounds can be satisfied for all times. A more relaxed (and realistic) assumption would be ultimate boundedness of the inner-loop tracking errors; under this

assumption, the results in this paper would still hold with a few modifications, especially affecting the initial transient phase. For simplicity, however, we assume that the performance bounds in Eqs. (9) and (11) hold uniformly in time. From a practical perspective, these performance bounds (as well as the constraints on them derived in the following sections) should be seen as guidelines/specifications for the design of the inner-loop autopilots.

III. Three-Dimensional Path Following for a Single Unmanned Aerial Vehicle

This section describes an outer-loop 3-D path-following nonlinear control algorithm that uses vehicle angular rates to steer the i th vehicle along the spatial path $p_{d,i}(\cdot)$ for an arbitrary feasible speed profile (temporal assignment along the path). Controller design builds on previous work by the authors on path-following control of small tactical UAVs, reported in [43], and derives new path-following control laws on SO(3) that avoid the geometric singularities and complexities that appear when dealing with local parameterizations of the vehicle's attitude or quaternions. First, only the kinematic equations of the UAV are addressed by taking pitch rate and yaw rate as virtual outer-loop control inputs. In particular, it is shown that there exist stabilizing functions for $q(t)$ and $r(t)$, leading to local exponential stability of the origin of \mathcal{G}_e with a prescribed domain of attraction. Then, a stability analysis is performed for the case of nonperfect inner-loop tracking, and it is shown that the path-following errors are locally uniformly ultimately bounded with the same domain of attraction. The results yield an efficient methodology to design path-following controllers for UAVs with due account for the vehicle kinematics and the characteristics of their inner-loop autopilots.

A. Nonlinear Control Design Using Unmanned Aerial Vehicle Kinematics

Recall from Sec. II.A that the main objective of the path-following control algorithm is to drive the position error $p_F(t)$ and the attitude error $e_{\tilde{R}}(t)$ to zero. At the kinematic level, these objectives can be achieved by determining feedback control laws for $q(t)$, $r(t)$, and $\ell(t)$ that ensure that the origin of the kinematic-error equations in Eq. (6) is exponentially stable with a given domain of attraction.

To solve the path-following problem, let the rate of progression of point P along the path be governed by

$$\dot{\ell} = (v\mathbf{w}_1 + K_\ell p_F) \cdot \mathbf{t} \quad (12)$$

where K_ℓ is a positive constant gain. Then, the rate commands $q_c(t)$ and $r_c(t)$ given by

$$\begin{bmatrix} q_c \\ r_c \end{bmatrix} \triangleq \Pi_R \tilde{R}^T (R_F^D \{\omega_{F/I}\}_F + \{\omega_{D/F}\}_D) - 2K_{\tilde{R}} e_{\tilde{R}} \quad (13)$$

where $K_{\tilde{R}}$ is also a positive constant gain, drive the path-following generalized error vector $x_{pf}(t)$ to zero with a guaranteed rate of convergence. A formal statement of this result is given in the next lemma.

Lemma 1: Assume that the UAV speed $v(t)$ verifies the following bounds:

$$0 < v_{\min} \leq v(t) \leq v_{\max}, \quad \forall t \geq 0 \quad (14)$$

If, for given positive constants $c < \frac{1}{\sqrt{2}}$ and c_1 , the path-following control parameters K_ℓ , $K_{\tilde{R}}$, and d are chosen such that

$$K_{\tilde{R}} K_p > \frac{v_{\max}^2}{c_1^2 (1 - 2c^2)^2} \quad (15)$$

where K_p is defined as

$$K_p \triangleq \min \left\{ K_\ell, \frac{v_{\min}}{(d^2 + c^2 c_1^2)^{\frac{1}{2}}} \right\} \quad (16)$$

then the rate commands in Eq. (13), together with the law in Eq. (12) for the rate of progression of the virtual target along the path, ensure

that the origin of the kinematic-error equations in Eq. (6) is exponentially stable with guaranteed rate of convergence

$$\begin{aligned} \bar{\lambda}_{pf} &\triangleq \frac{K_p + K_{\tilde{R}}(1 - c^2)}{2} \\ &- \frac{1}{2} \left((K_p - K_{\tilde{R}}(1 - c^2))^2 + \frac{4(1 - c^2)}{c_1^2(1 - 2c^2)^2} v_{\max}^2 \right)^{\frac{1}{2}} \end{aligned} \quad (17)$$

and domain of attraction

$$\Omega_c \triangleq \left\{ (p_F, \tilde{R}) \in \mathbb{R}^3 \times \text{SO}(3) \mid \Psi(\tilde{R}) + \frac{1}{c_1^2} \|p_F\|^2 \leq c^2 < \frac{1}{2} \right\} \quad (18)$$

Proof: A sketch of the proof of this result, which uses some insight from [52], is given in Appendix B.

Remark 2: The choice of the characteristic distance d in the definition of the auxiliary frame \mathcal{D} [see Eq. (2)] can be used to adjust the rate of convergence for the path-following closed-loop system. This is consistent with the fact that a large parameter d reduces the penalty for cross-track position errors, which results in a small rate of convergence of the UAV to the path. Insights into this path-following control algorithm can be found in [53].

B. Stability Analysis for Nonperfect Inner-Loop Tracking

The stabilizing control laws in Eqs. (12) and (13) lead to local exponential stability of the origin of the path-following kinematic-error dynamics [Eq. (6)] with a prescribed domain of attraction. In general, this result does not hold when the dynamics of the UAV are included in the problem formulation. This section presents a stability analysis of the path-following closed-loop system for the case of nonideal inner-loop tracking. In particular, it is assumed that the onboard autopilot ensures that the UAV is able to track bounded pitch-rate and yaw-rate commands with the performance bounds in Eq. (9) and show that the path-following errors $p_F(t)$ and $e_{\tilde{R}}(t)$ are locally uniformly ultimately bounded with the same domain of attraction Ω_c . The next lemma states this result formally.

Lemma 2: Assume that the UAV speed $v(t)$ verifies the bounds in Eq. (14). For given positive constants $c < \frac{1}{\sqrt{2}}$ and c_1 , choose the path-following control parameters K_ℓ , $K_{\tilde{R}}$, and \bar{d} according to the design constraint in Eq. (15). Further, let $\lambda_{pf} \triangleq \bar{\lambda}_{pf}(1 - \delta_\lambda)$, where $\bar{\lambda}_{pf}$ was defined in Eq. (17) and δ_λ is a positive constant verifying $0 < \delta_\lambda < 1$. If the performance bounds γ_q and γ_r in Eq. (9) satisfy the following inequality:

$$\gamma_\omega \triangleq (\gamma_q^2 + \gamma_r^2)^{\frac{1}{2}} < \frac{2c}{(1 - c^2)^{\frac{1}{2}}} \bar{\lambda}_{pf} \delta_\lambda \quad (19)$$

then, for any initial state $(p_F(0), \tilde{R}(0)) \in \Omega_c$, the rate commands in Eq. (13), together with the law in Eq. (12) for the rate of progression of the virtual target along the path, ensure that there is a time $T_b \geq 0$ such that the path-following errors $p_F(t)$ and $e_{\tilde{R}}(t)$ satisfy

$$\begin{aligned} \|e_{\tilde{R}}(t)\|^2 + \frac{1}{c_1^2} \|p_F(t)\|^2 &\leq \left(\frac{1}{1 - c^2} \|e_{\tilde{R}}(0)\|^2 + \frac{1}{c_1^2} \|p_F(0)\|^2 \right) e^{-2\lambda_{pf} t}, \\ \forall 0 \leq t < T_b \end{aligned} \quad (20)$$

$$\|e_{\tilde{R}}(t)\|^2 + \frac{1}{c_1^2} \|p_F(t)\|^2 \leq \frac{(1 - c^2)\gamma_\omega^2}{4\bar{\lambda}_{pf}^2 \delta_\lambda^2}, \quad \forall t \geq T_b \quad (21)$$

Proof: A sketch of the proof of this result is given in Appendix C.

Remark 3: Equations (20) and (21) show that the path-following errors $p_F(t)$ and $e_{\tilde{R}}(t)$ are uniformly bounded for all $t \geq 0$ and uniformly ultimately bounded with ultimate bounds:

$$\|e_{\tilde{R}}(t)\| \leq \frac{(1 - c^2)^{\frac{1}{2}}}{2\bar{\lambda}_{pf} \delta_\lambda} \gamma_\omega, \quad \|p_F(t)\| \leq \frac{c_1(1 - c^2)^{\frac{1}{2}}}{2\bar{\lambda}_{pf} \delta_\lambda} \gamma_\omega, \quad \forall t \geq T_b$$

These ultimate bounds are proportional to the inner-loop tracking performance bound γ_ω and, in the limit ideal case of perfect inner-loop tracking, one recovers the exponential stability result derived in Lemma 1.

Remark 4: An implicit assumption in the previous derivations is that the presence of wind (and gusts) does not result in the UAV flying at zero or “negative” ground speed. This assumption also holds throughout the remainder of the paper for all of the UAVs involved in the cooperative mission. In the case of strong winds that would violate this assumption, trajectory replanning will be required.

IV. Time-Critical Coordination

The previous section offered a solution to the path-following problem for a single vehicle and an arbitrary feasible speed profile by using a control strategy in which the vehicle’s attitude-control effectors are used to follow a virtual target running along the path. The problem of time-critical cooperative control of multiple vehicles is now addressed. To this effect, the speeds of the vehicles are adjusted based on coordination information exchanged among the vehicles over a time-varying network. In particular, the outer-loop coordination control law is intended to provide a correction to the desired speed profile $v_{d,i}(\cdot)$ obtained in the trajectory-generation step and to generate a total speed command $v_{c,i}(t)$. This speed command is then to be tracked by the i th vehicle to achieve coordination in time.

Recall from Sec. II.B that the main objective of the time-critical cooperative algorithm is to drive the coordination errors $|\xi_i(t) - \xi_j(t)|$ to a neighborhood of the origin. To solve this coordination problem, note that, from the definitions of $\ell'_{d,i}(\cdot)$ and $\eta_i(\cdot)$, it follows that the time derivative of the i th coordination state can be expressed as

$$\dot{\xi}_i(t) = \frac{\dot{\ell}_i(t)}{v_{d,i}(\xi_i(t))}$$

Next, recall from the solution to the path-following problem that the evolution of the i th virtual target vehicle along the path is given by $\dot{\ell}_i = (v_i \mathbf{w}_{1,i} + K_\ell p_{F,i}) \cdot \mathbf{t}_i$, where for simplicity K_ℓ has been kept without indexing and the dependency of the various variables on t has been dropped. The dynamics of the i th coordination state can thus be rewritten as

$$\dot{\xi}_i = \frac{(v_i \mathbf{w}_{1,i} + K_\ell p_{F,i}) \cdot \mathbf{t}_i}{v_{d,i}(\xi_i)} \quad (22)$$

At this point, it is important to remark that, if the path-following control law can guarantee that, for every UAV, the quantity $(\mathbf{w}_{1,i} \cdot \mathbf{t}_i)$ is positive and bounded away from zero for all $t \geq 0$, that is,

$$\mathbf{w}_{1,i} \cdot \mathbf{t}_i \geq c_2 > 0, \quad \forall t \geq 0, \quad \forall i \in \{1, \dots, n\} \quad (23)$$

where $0 < c_2 \leq 1$; then, to solve the coordination problem, one can use dynamic inversion and define the speed command for the i th vehicle as

$$v_{c,i} \triangleq \frac{u_{\text{coord},i} v_{d,i}(\xi_i) - K_\ell p_{F,i} \cdot \mathbf{t}_i}{\mathbf{w}_{1,i} \cdot \mathbf{t}_i} \quad (24)$$

where $u_{\text{coord},i}(t)$ is a coordination control law, yet to be defined. With this speed command, the dynamics of the i th coordination state [Eq. (22)] can be rewritten as

$$\dot{\xi}_i = u_{\text{coord},i} + \frac{e_{v,i}}{v_{d,i}(\xi_i)} \mathbf{w}_{1,i} \cdot \mathbf{t}_i \quad (25)$$

where $e_{v,i}(t) \triangleq v_i(t) - v_{c,i}(t)$ denotes the velocity tracking error for the i th vehicle. In what follows, it is assumed that the bound in Eq. (23) holds for every vehicle, and a coordination control law $u_{\text{coord},i}(t)$ is derived that achieves coordination for the entire fleet of UAVs. This assumption will be verified later in Sec. V, where stability

of the combined time-critical cooperative path-following closed-loop system is proven and an expression for the constant c_2 is derived.

Recall now that each vehicle is allowed to exchange only its coordination parameter $\xi_i(t)$ with its neighbors \mathcal{N}_i , which are defined by the time-varying communications topology. To observe this constraint, the following distributed coordination law is proposed:

$$u_{\text{coord},1}(t) = -a \sum_{j \in \mathcal{N}_1} (\xi_1(t) - \xi_j(t)) + 1 \quad (26a)$$

$$u_{\text{coord},i}(t) = -a \sum_{j \in \mathcal{N}_i} (\xi_i(t) - \xi_j(t)) + \chi_{I,i}(t), \quad i = 2, \dots, n \quad (26b)$$

$$\dot{\chi}_{I,i}(t) = -b \sum_{j \in \mathcal{N}_i} (\xi_i(t) - \xi_j(t)), \quad \chi_{I,i}(0) = 1, \quad i = 2, \dots, n \quad (26c)$$

where vehicle 1 is elected as the formation leader (which can be a virtual vehicle), and a and b are positive adjustable coordination control gains. Note that the coordination control law has a proportional-integral structure, which provides disturbance rejection capabilities at the coordination level. Moreover, note that the vehicles exchange information only about the corresponding virtual targets, rather than exchanging their own state information.

The coordination law in Eq. (26) can be rewritten in compact form as

$$\begin{aligned} u_{\text{coord}}(t) &= -a L(t) \xi(t) + \begin{bmatrix} 1 \\ \chi_I(t) \end{bmatrix}, \\ \dot{\chi}_I(t) &= -b C^T L(t) \xi(t), \quad \chi_{I,i}(0) = 1 \end{aligned} \quad (27)$$

where $\xi(t) \triangleq [\xi_1(t), \dots, \xi_n(t)]^T$, $u_{\text{coord}}(t) \triangleq [u_{\text{coord},1}(t), \dots, u_{\text{coord},n}(t)]^T$, $\chi_I(t) \triangleq [\chi_{I,2}(t), \dots, \chi_{I,n}(t)]^T$, $C^T \triangleq [0 \ \mathbb{I}_{n-1}]$, and $L(t)$ is the Laplacian of the undirected graph $\Gamma(t)$ that captures the underlying bidirectional communications network topology of the UAV formation at time t . It is well known that the Laplacian of an undirected graph is symmetric, $L^T(t) = L(t)$, and positive semidefinite, $L(t) \geq 0$; $\lambda_1(L(t)) = 0$ is an eigenvalue with eigenvector 1_n , $L(t)1_n = 0$; and the second smallest eigenvalue of $L(t)$ is positive if and only if the graph $\Gamma(t)$ is connected.

Next, the coordination problem stated previously is reformulated into a stabilization problem. To this end, define the projection matrix Π as $\Pi \triangleq \mathbb{I}_n - \frac{1}{n} 1_n 1_n^T$, and note that $\Pi = \Pi^T = \Pi^2$ and also that $Q^T Q = \Pi$, where Q is the $(n-1) \times n$ matrix introduced in Eq. (8). Moreover, one has that $L(t)\Pi = \Pi L(t) = L(t)$, and the spectrum of the matrix $\bar{L}(t) \triangleq Q L(t) Q^T$ is equal to the spectrum of $L(t)$ without the eigenvalue $\lambda_1 = 0$ corresponding to the eigenvector 1_n . Finally, define the coordination error state $\zeta(t) \triangleq [\zeta_1(t)^T, \zeta_2(t)^T]^T$ as

$$\zeta_1(t) \triangleq Q \xi(t) \quad \zeta_2(t) \triangleq \chi_I(t) - 1_{n-1}$$

By definition, $\zeta_1(t) = 0$ is equivalent to $\xi(t) \in \text{span}\{1_n\}$, which implies that, if $\zeta(t) = 0$, then all target vehicles are coordinated at time t .

With the previous notation, the closed-loop coordination dynamics formed by Eq. (25) and the coordination control algorithm defined in Eq. (27) can be reformulated as

$$\dot{\zeta}(t) = F(t) \zeta(t) + H e_v'(t) \quad (28)$$

where $F(t) \in \mathbb{R}^{(2n-2) \times (2n-2)}$ and $H \in \mathbb{R}^{(2n-2) \times n}$ are given by

$$F(t) \triangleq \begin{bmatrix} -a \bar{L}(t) & QC \\ -b C^T Q^T \bar{L}(t) & 0 \end{bmatrix}, \quad H \triangleq \begin{bmatrix} Q \\ 0 \end{bmatrix}$$

and $e'_v(t) \in \mathbb{R}^n$ is a vector with its i th component equal to $e'_{v,i} \triangleq \frac{e_{v,i}}{v_{d,i}(\xi_i)} \mathbf{w}_{1,i} \cdot \mathbf{t}_i$.

Next, it is shown that, if the connectivity of the communications graph $\Gamma(t)$ verifies the PE-like condition of Eq. (8) and, in addition, every vehicle travels at the commanded speed $v_{c,i}(t)$, that is $e_{v,i}(t) \equiv 0$, then the coordinated system asymptotically reaches agreement and all the vehicles travel at the desired speed

$$\lim_{t \rightarrow \infty} (\xi_i(t) - \xi_j(t)) = 0, \quad \forall i, j \in \{1, \dots, n\}$$

$$\lim_{t \rightarrow \infty} \dot{\xi}(t) = 1_n$$

On the other hand, if $e_{v,i}(t) \neq 0$ for some $t \geq 0$, then the coordination error vector degrades gracefully with the size of the speed-tracking error $e_v(t) \triangleq [e_{v,1}(t), \dots, e_{v,n}(t)]^T$. The next lemma summarizes this result.

Lemma 3: Consider the coordination system of Eq. (28) and suppose that the Laplacian of the graph that models the communications topology satisfies the PE-like condition of Eq. (8) for some parameters μ and T . Moreover, assume that the speed-tracking error vector $e_v(t)$ is bounded for all $t \geq 0$. Then, there exist coordination control gains a and b such that the system [Eq. (28)] is input-to-state stable (ISS) with respect to $e_v(t)$, satisfying

$$\|\zeta(t)\| \leq k_1 \|\zeta(0)\| e^{-\lambda_c t} + k_2 \sup_{\tau \in [0,t]} \|e_v(\tau)\|, \quad \forall t \geq 0 \quad (29)$$

for some positive constants $k_1, k_2 \in (0, \infty)$, and with $\lambda_c \triangleq \bar{\lambda}_c(1 - \theta_\lambda)$, where

$$\bar{\lambda}_c \triangleq \frac{a n \mu}{(1 + a n T)^2} (1 + \beta)^{-1}, \quad \beta \geq 2n, \quad \text{and} \quad 0 < \theta_\lambda < 1$$

Furthermore, the coordination states $\xi_i(t)$ and their rates of change $\dot{\xi}_i(t)$ satisfy

$$\limsup_{t \rightarrow \infty} |\xi_i(t) - \xi_j(t)| \leq k_3 \limsup_{t \rightarrow \infty} \|e_v(t)\| \quad (30)$$

$$\limsup_{t \rightarrow \infty} |\dot{\xi}_i(t) - 1| \leq k_4 \limsup_{t \rightarrow \infty} \|e_v(t)\| \quad (31)$$

for all $i, j \in \{1, \dots, n\}$ and for some positive constants $k_3, k_4 \in (0, \infty)$.

Proof: A sketch of the proof of this result is given in Appendix D.

Remark 5: Lemma 3 indicates that the QoS of the network (characterized by parameters T and μ) limits the achievable (guaranteed) rate of convergence for the coordination control loop. According to the lemma, for a given QoS of the network, the maximum upper bound on the (guaranteed) rate of convergence $\bar{\lambda}_c^*$ is achieved by setting $a^* = (1/Tn)$, which results in $\bar{\lambda}_c^* = \frac{\mu}{4T}(1 + \beta)^{-1}$. Also, it is important to mention that, as the parameter T goes to zero (graph connected pointwise in time), the upper bound on the convergence rate can be set arbitrarily fast by increasing the coordination control gains a and b . This is consistent with results obtained in previous work by the authors (see [40], Lemma 2).

Finally, notice that $\bar{\gamma}_\lambda \triangleq [an\mu/(1 + a n T)^2]^2$ represents the upper bound on the (guaranteed) convergence rate for the coordination loop with a proportional control law, rather than a proportional-integral control law (see Appendix D). It is straightforward to verify that, for a given proportional gain a , one has that $\bar{\lambda}_c < \bar{\gamma}_\lambda$, which implies that a proportional control law can provide higher rates of convergence than the proportional-integral control law used in this paper. However, as mentioned earlier, the integral term in the coordination control law is important in the current application because it provides disturbance rejection capabilities at the coordination level; see [54].

V. Combined Path Following and Time-Critical Cooperation

The previous sections have shown that, under an appropriate set of assumptions, the path-following and coordination control laws are able to ensure stability and ultimate boundedness of the path-following and time-critical cooperation problems when treated separately. In particular, the solution developed for the path-following problem assumes that the speed of the UAV is bounded above and below, while the control law designed for vehicle coordination relies on the assumption that the angle between the UAV's velocity vector and the tangent direction to the path is less than 90 deg; see Eqs. (14) and (23). This section addresses the convergence properties of the combined cooperation and path-following systems and derives design constraints for the inner-loop tracking performance bounds that guarantee stability of the complete system. The cooperative path-following control architecture for the i th UAV is presented in Fig. 2.

In this section, it is assumed that the onboard autopilot ensures that each UAV is able to track bounded pitch-rate, yaw-rate, and speed commands with the performance bounds in Eqs. (9)–(11). Note that, although the pitch-rate and yaw-rate commands in Eq. (13) are continuous in time, the same cannot be said about the speed command in Eq. (24). In fact, because of the time-varying nature of the network topology, the coordination law $u_{\text{coord}}(t)$ in Eq. (26) is discontinuous, which implies that the speed command $v_c(t)$ is also discontinuous. Assuming that the following bound holds for all vehicles and for all $t \geq 0$,

$$|v_{c,i}(t) - v_i(t)| \leq \gamma_v, \quad i = 1, \dots, n \quad (32)$$

which implies that $\sup_{t \geq 0} \|e_v(t)\| \leq \sqrt{n}\gamma_v$, then the maximum amplitude $\Delta v_{c,i}$ of a jump in the speed command $v_{c,i}(t)$ can be derived from Eqs. (24) and (26) and the results of Lemma 3 and is given by

$$\Delta v_{c,i} \triangleq \frac{2a(n-1)v_{d,i} \max(k_1 \|\zeta(0)\| + k_2 \sqrt{n}\gamma_v)}{c_2}, \quad i = 1, \dots, n$$

where $v_{d,i} \max$ was introduced in Eq. (7). Thus, a necessary (but by no means sufficient) condition for the bound in Eq. (32) to hold is that

$$\Delta v_{c,i} < \gamma_v, \quad i = 1, \dots, n$$

The previous condition limits the choice of the coordination control gains, which in particular need to satisfy the following inequality

$$2a(n-1)v_{d,i} \max k_2 \sqrt{n} < c_2, \quad i = 1, \dots, n$$

However, the derivation of sufficient conditions that guarantee that the bound in Eq. (11) holds for all time requires assumptions on

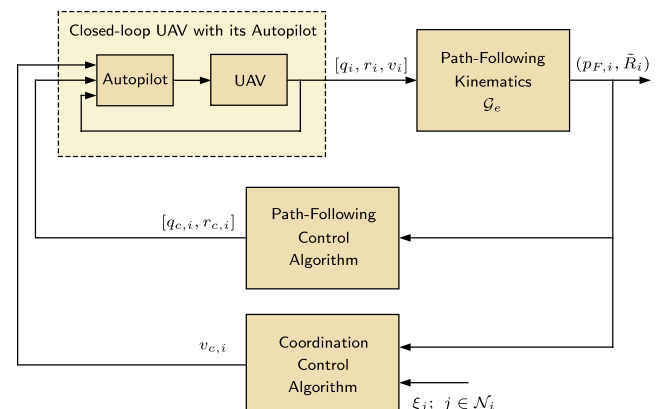


Fig. 2 Time-critical cooperative path-following closed-loop for the i th vehicle.

vehicle dynamics and autopilot design and is thus beyond the scope of this paper. Hence, for the subsequent developments, the assumption is made that the bound in Eq. (11) holds, provided that the speed command $v_{c,i}(t)$ satisfies the bounds in Eq. (10), and design constraints for this inner-loop tracking performance bound are derived that ensure that the overall time-critical cooperative path-following control system is stable and has desired convergence properties. The next theorem summarizes this result.

Theorem 1: Consider a fleet of n UAVs supported by a communications network that satisfies the PE-like condition in Eq. (8). Let c and c_1 be positive constants, with $c < (1/\sqrt{2})$ and $c_1 < (E/c)$. For each UAV, choose the path-following control parameters K_ℓ , $K_{\tilde{R}}$, and d such that

$$d > \frac{2c(1 - c^2)^{\frac{1}{2}}}{1 - 2c^2} c_1, \quad K_{\tilde{R}} K_p > \frac{v_{\max}^2}{c_1^2(1 - 2c^2)^2} \quad (33)$$

where K_p is defined as in Eq. (16). Also, choose the coordination control gains a and b such that

$$a > 0, \quad \frac{2n}{2n + 1} \frac{an\mu}{(1 + anT)^2} \leq \frac{b}{a} \leq \frac{an\mu}{(1 + anT)^2} \quad (34)$$

and let k_1 and k_2 be the constants in Eq. (29) for this particular choice of control gains a and b . Further, let the performance bounds γ_q , γ_r , and γ_v satisfy the following inequalities:

$$(\gamma_q^2 + \gamma_r^2)^{\frac{1}{2}} < \frac{2c}{(1 - c^2)^{\frac{1}{2}}} \bar{\lambda}_{pf} \delta_\lambda \quad (35)$$

$$\gamma_v < \min \left\{ \frac{v_{\max} c_2 - v_{d,\max} - K_\ell c c_1}{c_2 + \bar{k}_2 v_{d,\max} \sqrt{n}}, \frac{v_{d,\min} - v_{\min} - K_\ell c c_1}{1 + \bar{k}_2 v_{d,\max} \sqrt{n}} \right\} \quad (36)$$

where δ_λ is a constant satisfying $0 < \delta_\lambda < 1$, $v_{d,\max} \triangleq \max_{i=1,\dots,n} v_{d,i,\max}$, $v_{d,\min} \triangleq \min_{i=1,\dots,n} v_{d,i,\min}$, while c_2 and \bar{k}_2 are defined as $c_2 \triangleq [d(1 - 2c^2) - 2c_1 c^2 (1 - c^2)^{\frac{1}{2}}]/[(d^2 + c^2 c_1^2)^{\frac{1}{2}}]$ and $\bar{k}_2 \triangleq (2a(n-1) + 1)k_1$. Then, the progression law in Eq. (12), the rate commands in Eq. (13), and the speed commands in Eq. (24) with the coordination control law in Eq. (26) ensure that, for all initial conditions

$$(p_{F,i}(0), \tilde{R}_i(0)) \in \Omega_c, \quad i = 1, \dots, n \quad (37)$$

$$\begin{aligned} \|\zeta(0)\| &\leq \frac{1}{k_1} \left(\min \left\{ \frac{v_{\max} - \gamma_v}{v_{d,\max}} c_2 - 1, \frac{v_{d,\min} - v_{\min} + \gamma_v}{v_{d,\max}} \right\} \right. \\ &\quad \left. - \bar{k}_2 \sqrt{n} \gamma_v - \frac{K_\ell c c_1}{v_{d,\max}} \right) \end{aligned} \quad (38)$$

where $\bar{k}_1 \triangleq (2a(n-1) + 1)k_1$, there exist times $T_{b,i} \geq 0$ and a positive constant λ_c such that the path-following errors $p_{F,i}(t)$ and $e_{\tilde{R},i}(t)$ for the i th UAV satisfy

$$\begin{aligned} &\|e_{\tilde{R},i}(t)\|^2 + \frac{1}{c_1^2} \|p_{F,i}(t)\|^2 \\ &\leq \left(\frac{1}{1 - c^2} \|e_{\tilde{R},i}(0)\|^2 + \frac{1}{c_1^2} \|p_{F,i}(0)\|^2 \right) e^{-2\bar{\lambda}_{pf}(1-\delta_\lambda)t}, \\ &\forall 0 \leq t < T_{b,i} \end{aligned} \quad (39)$$

$$\|e_{\tilde{R},i}(t)\|^2 + \frac{1}{c_1^2} \|p_{F,i}(t)\|^2 \leq \frac{(1 - c^2)\gamma_v^2}{4\bar{\lambda}_{pf}^2 \delta_\lambda^2}, \quad \forall t \geq T_{b,i} \quad (40)$$

while the coordination error states $\zeta(t)$ satisfy

$$\|\zeta(t)\| \leq k_1 \|\zeta(0)\| e^{-\lambda_c t} + k_2 \sqrt{n} \gamma_v, \quad \forall t \geq 0 \quad (41)$$

Proof: A sketch of the proof of this result is given in Appendix E.

Remark 6: The previous lemma shows that, if the initial conditions for each UAV satisfy Eq. (37), then the UAVs remain inside tubes of radii $c c_1$ centered at the corresponding desired paths during the entire duration of the mission. The bound $c_1 < E/c$, where E is the spatial clearance between paths introduced at the beginning of Sec. II, ensures that these tubes do not intersect and, hence, the UAVs do not collide. In the case of collision avoidance in time (see [44]), the bound on c_1 is more involved and accounts for both path-following and coordination errors.

Remark 7: Equations (39, 40) show that the path-following errors $p_{F,i}(t)$ and $e_{\tilde{R},i}(t)$ are uniformly bounded for all $t \geq 0$ and uniformly ultimately bounded with ultimate bounds

$$\begin{aligned} \|e_{\tilde{R},i}(t)\| &\leq \frac{(1 - c^2)^{\frac{1}{2}}}{2\bar{\lambda}_{pf} \delta_\lambda} \gamma_\omega, \\ \|p_{F,i}(t)\| &\leq \frac{c_1(1 - c^2)^{\frac{1}{2}}}{2\bar{\lambda}_{pf} \delta_\lambda} \gamma_\omega, \quad \forall t \geq T_b, \quad \forall i \in \{1, \dots, n\} \end{aligned}$$

which are proportional to the inner-loop tracking performance bound γ_ω . On the other hand, Eq. (41) implies that the coordination error state $\zeta(t)$ converges exponentially fast to a neighborhood of the origin with radius proportional to the inner-loop speed-tracking performance bound γ_v . This implies that, in the limit case of perfect inner-loop tracking, the path-following errors of each vehicle and the coordination error state vector converge exponentially fast to zero.

Remark 8: The design constraint in Eq. (36) requires a sufficiently large margin between $v_{d,\max}$ and v_{\max} and between $v_{d,\min}$ and v_{\min} . This can be achieved by directly imposing tighter feasibility constraints on vehicle's speed in the formulation of the trajectory-generation problem; see [44].

VI. Cooperative Road Search with Multiple Unmanned Aerial Vehicles

This section presents flight-test results for a cooperative road-search mission that show the efficacy of the multi-UAV cooperative framework presented in this paper. The significance of these experiments is twofold. First, the flight-test results verify the main stability and convergence properties of the developed cooperative algorithms in a realistic mission scenario, under environmental disturbances and with the limitations of a real-world communications network. And second, the results demonstrate the usefulness and validity of the proposed generic theoretical framework in a specific realistic application as well as the feasibility of the onboard implementation of the algorithms. More flight tests are scheduled in 2013 to conduct a more thorough verification of the theoretical findings of this paper.

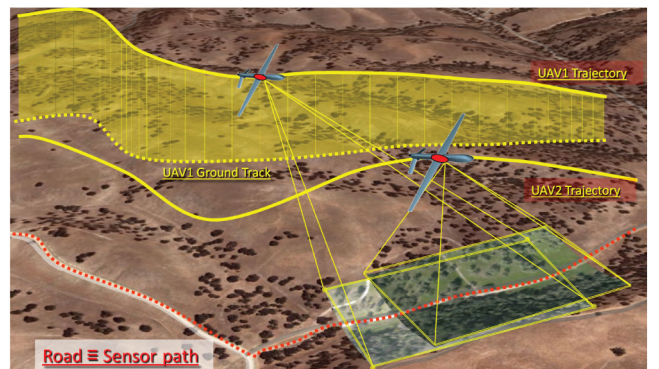


Fig. 3 The concept of coordinated road search using multiple UAVs.

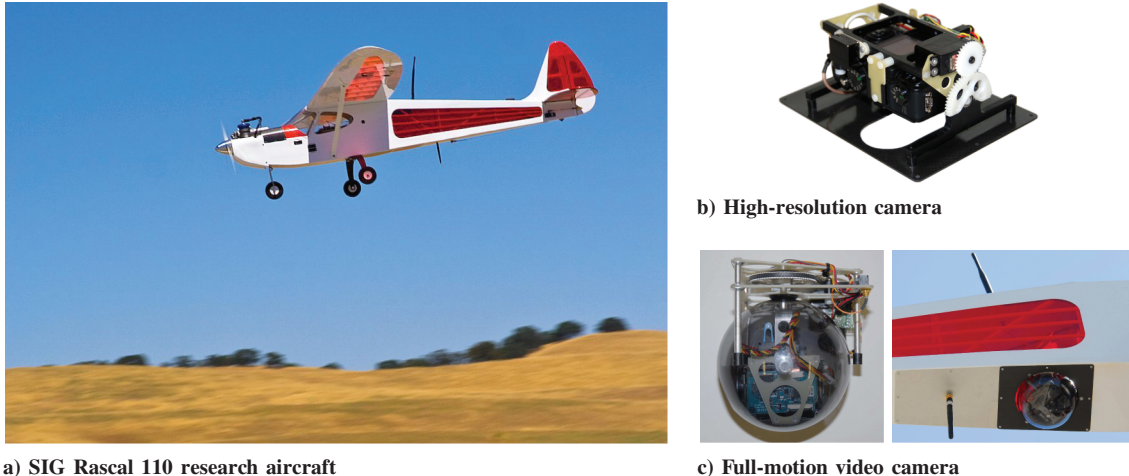


Fig. 4 SIG Rascal UAV with two different onboard cameras.

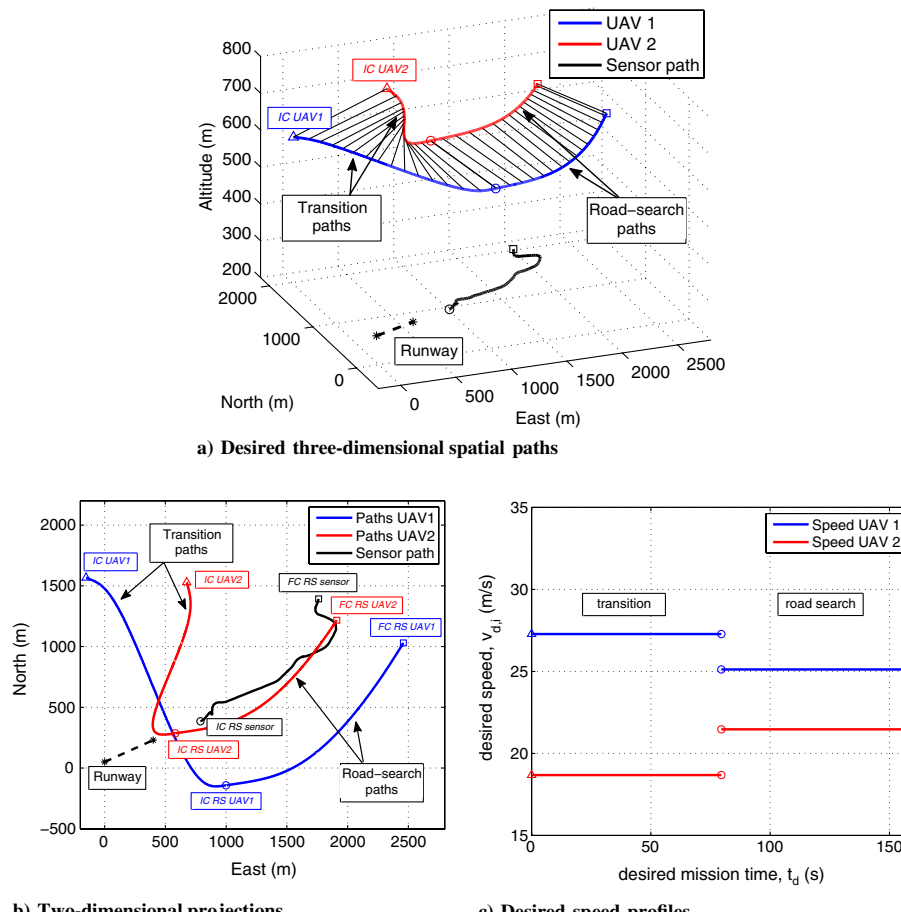


Fig. 5 Coordinated road-search trajectory generation.

A. Mission Description

One of the applications that motivates the use of multiple cooperative UAVs and poses several challenges to systems engineers, both from a theoretical and practical standpoint, is automatic road search for improvised explosive device detection; see Fig. 3. It is envisioned that the mission is initiated by a minimally trained user who scribbles a path on a digital map, generating a precise continuous ground track for the airborne sensors to follow. This ground track is then transmitted over the network to a fleet of small tactical UAVs equipped with complementary visual sensors. An optimization algorithm generates feasible collision-free flight trajectories that maximize road coverage and account for sensor capabilities (field of

view, resolution, and gimbal constraints) as well as intervehicle and ground-to-air communications limitations. Maximization of the road coverage by two complementary sensors is the high-level mission objective in this scenario. The fleet of UAVs then starts the cooperative road search. During this phase, the information obtained from the sensors mounted onboard the UAVs is shared over the network and retrieved by remote users in near real time. The explosive device detection can thus be done remotely, based on in situ imagery data delivered over the network.

In this particular mission scenario, a robust cooperative control algorithm for the fleet of UAVs can improve mission performance and provide reliable target discrimination by effectively combining

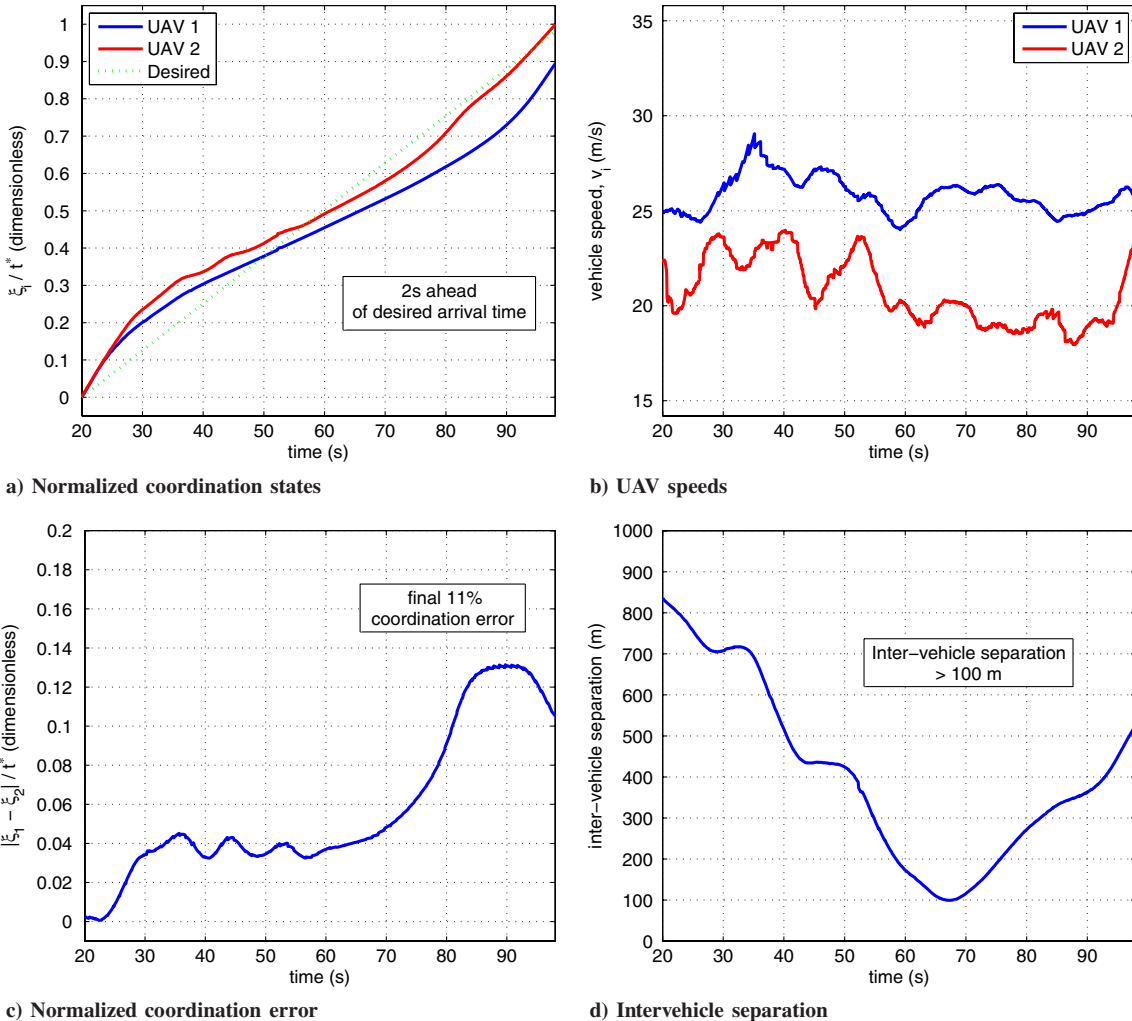


Fig. 6 Time coordination during the transition phase.

the capabilities of the complementary onboard sensors. In fact, flying in a coordinated fashion is what allows maximizing the overlap of the fields of view (FOVs) of multiple sensors while reliably maintaining a desired image resolution. Furthermore, this autonomous multivehicle cooperative approach can potentially reduce the number of operators involved in the mission as well as their workload.

B. Airborne System Architecture

The small tactical UAVs employed in this mission are two SIG Rascals 110 s operated by the Naval Postgraduate School; see Fig. 4. The two UAVs have identical avionics and instrumentation onboard, the only difference being the vision sensors. The first UAV has a one-degree-of-freedom bank-stabilized high-resolution 12 MP camera, while the second UAV has a full-motion video camera suspended on a two-degree-of-freedom pan-tilt gimbal. Because of weight and power constraints, each UAV is allowed to carry only one camera at a time, and therefore the two cameras need to be mounted on different platforms. The rest of the onboard avionics, common to both platforms, includes two PC-104 industrial embedded computers^{††} assembled in a stack, a wireless mobile ad hoc network (MANET) link^{***}, and the Piccolo Plus autopilot^{†††} with its dedicated 900 MHz command and control channel.

^{††}Data available online at <http://www.adl-usa.com/products/cpu/index.php> [retrieved 30 March 2012].

^{***}Data available online at <http://www.persistentsystems.com> [retrieved 30 March 2012].

^{†††}Data available online at <http://cloudcaptech.com> [retrieved 30 March 2012].

The first PC-104 computer runs the cooperative-control algorithms in hard real time at 100 Hz. The computer directly communicates with the Piccolo Plus autopilot at 50 Hz over a dedicated bidirectional serial link. The second PC-104 acts as a mission management computer that implements a set of non-real-time routines enabling onboard preprocessing and retrieval of the sensory data (high-resolution imagery or video) in near-real time over the network. Integration of the MANET link allows for robust transparent intervehicle and ground communication, which is needed for both the coordination algorithms and the expedited sensory data delivery to a remote mission operator. In fact, the MANET link provides "any-to-any" connectivity capability, allowing every node (vehicle or ground station) to securely communicate directly with every other node. Details on the flight-test architecture and the supporting network infrastructure for coordination control and data dissemination can be found in [55].

C. Flight-Test Results

The flight-test results for a cooperative road-search mission executed by the two SIG Rascal UAVs are presented next. The objective of the mission is to detect a stationary or moving target on a given road. The imagery data obtained by the UAVs during the road search is to be shared over a MANET link so that it can be retrieved by remote operators in near real time. Success of the mission relies on the ability to overlap the footprint of the FOVs of the two cameras along the road, which increases the probability of target detection [56]. For the sake of clarity, in the following description, the execution of the coordinated road search is divided into three consecutive phases: namely initialization, transition, and road search. The description is supported by one of the flight-test results performed during a Tactical

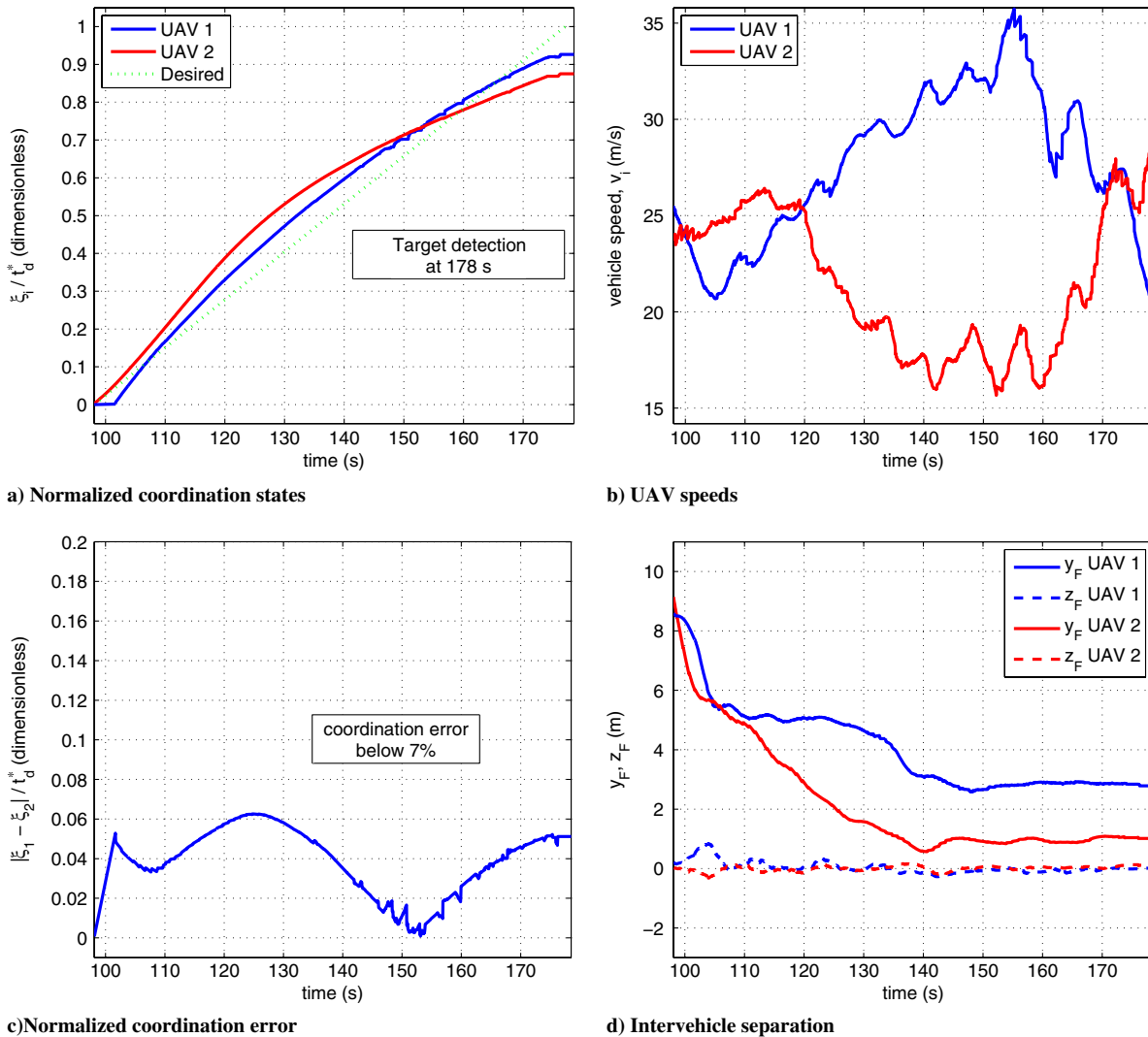


Fig. 7 Cooperative path-following control during the road-search phase.

Network Testbed field experiment at Camp Roberts, CA; see Figs. 5–8. These experimental results build on the ones reported in [44] by analyzing in greater detail the performance of the cooperative algorithms during the road-search phase.

In the initialization phase, an operator specifies on a digital map the road of interest. Then, a centralized optimization algorithm generates road-search suboptimal paths and desired speed profiles for the two UAVs that explicitly account for UAV dynamic constraints, collision-avoidance constraints, and mission-specific constraints such as intervehicle and vehicle-to-ground communications limitations as well as sensory capabilities. In particular, for this mission scenario, the trajectory-generation algorithm is designed to maximize the overlap of the footprints of the FOVs of the high-resolution camera and the full-motion video during the road search, while at the same time minimizing gimbal actuation. In addition to the road-search paths and the corresponding desired speed profiles, the outcome of the trajectory-generation algorithm includes a sensor trajectory on the ground to be followed by the vision sensors. The two road-search paths and the sensor path, along with the three corresponding speed profiles, are then transmitted to the UAVs over the MANET link.

In the transition phase, the two UAVs fly from their standby starting positions to the initial points of the respective road-search paths. For this purpose, decentralized optimization algorithms generate feasible collision-free 3-D trajectories that start at the UAVs' standby positions and satisfy simultaneous arrival to the initial points of the road-search paths. Once these transition trajectories are generated, the two vehicles start operating in cooperative path-following mode. From that moment on, the UAVs follow the

transition paths while adjusting their speeds based on coordination information exchanged over the MANET link to achieve simultaneous arrival at the starting point of the road-search paths. The transition and road-search paths obtained for this particular mission scenario, together with the corresponding desired speed profiles, are shown in Fig. 5. Figure 6 illustrates the performance of the coordination control algorithm during the transition phase of the mission. As can be observed, the intervehicle separation remains above 100 m and the coordination error remains below 13% during the entire duration of the transition phase, with an 11% error in coordination at the end of this phase.

Finally, the third phase addresses the cooperative road-search mission itself, in which the two UAVs follow the road-search paths generated in the initialization phase while adjusting their speeds to ensure the required overlap of the FOV footprints of the cameras. In this phase, a target vehicle running along the sensor path is virtually implemented on one of the UAVs. For this road-search mission, a natural choice for this sensor path is the road itself, and this virtual vehicle thus determines the spot of the road being observed by the vision sensors mounted onboard the UAVs at a given time. This virtual vehicle is indeed used as a leader in the coordination algorithm, and its speed is also adjusted, based on the coordination states of the two UAVs. The coordination state of this virtual vehicle is also transmitted over the network and used in the coordination control laws of the two “real” vehicles. The performance of the cooperative path-following control algorithm is illustrated in Fig. 7. For this particular scenario, the path-following cross-track errors converge to a 3 m tube around the desired spatial paths, while the

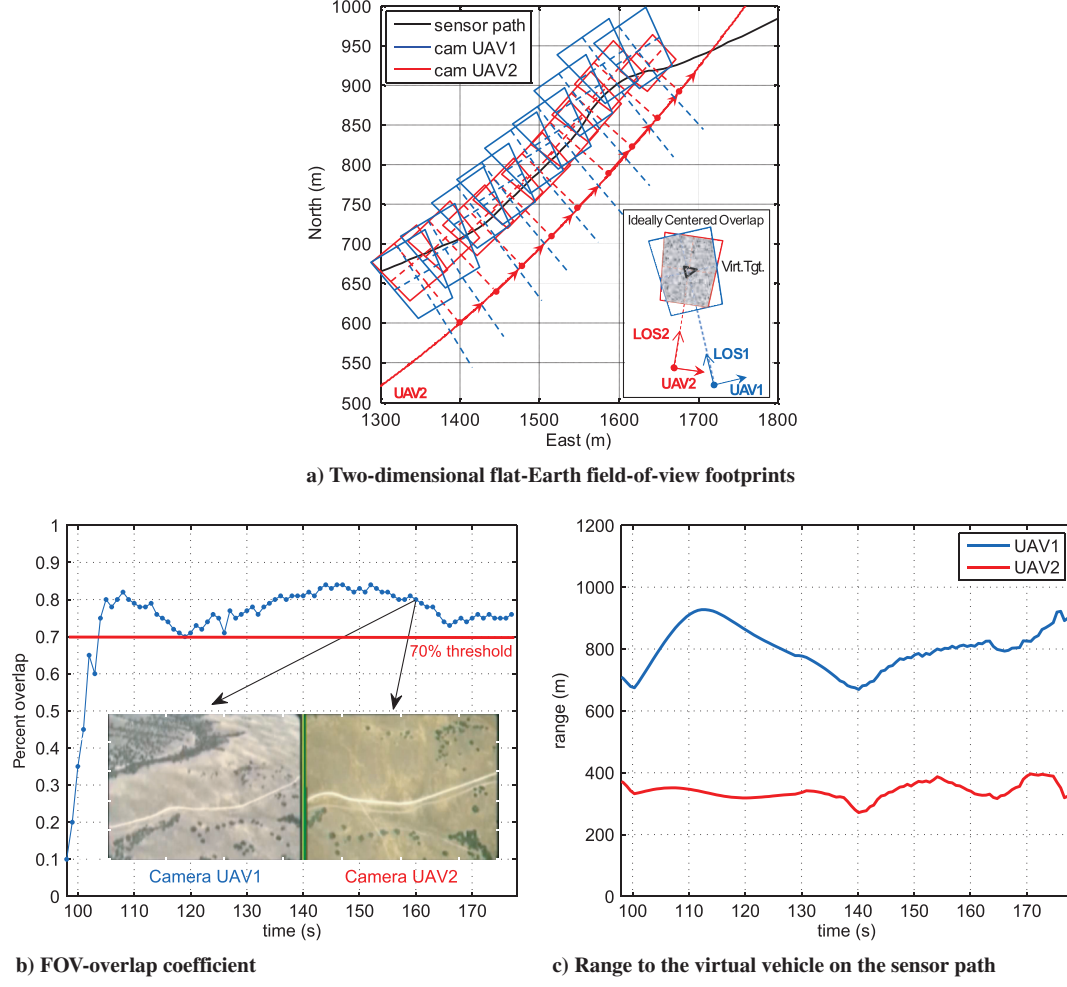


Fig. 8 Mission performance: FOV overlap and range to the virtual vehicle on the sensor path.

coordination errors remain below 7% during the entire duration of the road search. It is worth noting that significant data dropouts occurred between 145 s and 170 s, especially effecting UAV1; these data dropouts cause sudden jumps in the normalized coordination states, as can be seen in Figs. 7a and 7c. The road-search phase ends at 178 s, when a target is detected on the road. Upon detection, the two UAVs immediately switch to cooperative vision-based target-tracking mode. Flight-test results for this target-tracking phase are not included here and can be found in [44].

As mentioned previously, maintaining a tight coordination along the paths is important to ensure a desired level of FOV overlap with desired image resolution, two key elements for reliable target detection. Figure 8 illustrates the performance of the road-search mission from this perspective. One one hand, Fig. 8a shows a set of estimates of the ground FOV footprint, assuming a flat Earth with known ground elevation. These estimates assume a trapezoidal footprint and are based on experimental data including the inertial position and orientation of the two UAVs, orientation of their cameras, and the line-of-sight range to the ground. To provide a quantitative measure of the FOV overlap, Fig. 8b presents an image-overlap coefficient, sampled at 1 Hz. This coefficient is calculated offline using proprietary technology^{***} and is based on semi-automated alignment and differencing of two synchronous images. As can be seen, except for a 5 s initial transient, the overlap coefficient stays above 0.7 during the cooperative road search. This figure also includes a side-by-side image comparison of the imagery data obtained from the two cameras at approximately 160 s after initiation of the mission; one can easily observe that the two images correspond

to the same road segment. On the other hand, Fig. 8c shows the range for the two vision sensors to the virtual vehicle on the sensor path; these ranges are always below 1000 m for UAV1 and 500 m for UAV2, therefore ensuring desired image resolution for the targets of interest given the characteristics of the two cameras.

In summary, the results presented previously demonstrate feasibility and efficacy of the onboard integration of the nonlinear path-following and time-critical coordination algorithms. This cooperative control approach applies to teams of heterogeneous systems and does not necessarily lead to swarming behavior, which is unsuitable for many of the mission scenarios envisioned in this research. At the same time, the achieved functionality of the UAV following 3-D curves in an inertial space outperforms the conventional waypoint navigation method typically implemented on off-the-shelf commercial autopilots. These results provide also a roadmap for further development and onboard implementation of advanced cooperative algorithms.

VII. Conclusions

This paper addressed the problem of multiple unmanned aerial vehicle (UAV) cooperative control in the presence of time-varying communications networks and stringent spatial/temporal constraints. The constraints involve collision-free maneuvers and simultaneous times of arrival at desired target locations. The methodology proposed in the paper built on previous work by the authors on cooperative path following and extended it to a very general setting that allows for the consideration time-critical specifications and time-varying communications topologies. In the setup adopted, single-vehicle path-following control in three-dimensional space was done by resorting to a nonlinear control strategy derived at the kinematic level. Decentralized multiple-vehicle time-critical cooperative path

***Data available online at <http://perceptivu.com/TargetTrackingSoftware.html> [retrieved 4 September 2012].

following was achieved by adjusting the speed of each vehicle about a nominal speed profile, in response to information exchanged with its neighbors over a dynamic communications network. The proposed approach addressed explicitly the situation where each vehicle transmits only its coordination state to only a subset of the other vehicles, as determined by the communications topology adopted. Furthermore, the paper considered the case where the communications graph that captures the underlying communications network topology is disconnected during some interval of time or even fails to be connected for the entire duration of the mission, and it provided conditions under which the complete coordinated path-following closed-loop system is stable and yields convergence of conveniently defined cooperation error states to a neighborhood of the origin. The paper also derived lower bounds on the convergence rate of the collective dynamics as a function of the quality of service of the intervehicle communications network. Flight tests of a coordinated road-search mission scenario that exploited the multi-UAV cooperative control framework exposed in the paper demonstrated the efficacy of the algorithms developed. Future work will aim at extending the algorithms presented to other kinds of vehicles and maneuvers (e.g., quadrotor UAVs undergoing complex time-critical maneuvers that require synchronization of attitude and position).

Appendix A: Hat and Vee Maps

The hat map $(\cdot)^\wedge: \mathbb{R}^3 \rightarrow \mathfrak{so}(3)$ is defined as

$$(x)^\wedge = \begin{bmatrix} 0 & -x_3 & x_2 \\ x_3 & 0 & -x_1 \\ -x_2 & x_1 & 0 \end{bmatrix}$$

for $x = [x_1, x_2, x_3]^T \in \mathbb{R}^3$. The inverse of the hat map is referred to as the vee map $(\cdot)^\vee: \mathfrak{so}(3) \rightarrow \mathbb{R}^3$. A property of the hat and vee maps used in this paper is given next:

$$\text{tr}[M(x)^\wedge] = -x \cdot (M - M^T)^\vee \quad (\text{A1})$$

for any $x \in \mathbb{R}^3$, and $M \in \mathbb{R}^{3 \times 3}$. The reader is referred to [52] for further details on the hat and vee maps.

Appendix B: Sketch of the Proof of Lemma 1

First, note that, over the compact set Ω_c introduced in Eq. (18), the following upper bounds hold:

$$\|p_F\| \leq cc_1 < \frac{c_1}{\sqrt{2}} \quad (\text{B1})$$

$$\Psi(\tilde{R}) \leq c^2 < \frac{1}{2} \quad (\text{B2})$$

Consider now the Lyapunov function candidate

$$V_{pf}(p_F, \tilde{R}) = \Psi(\tilde{R}) + \frac{1}{c_1^2} \|p_F\|^2$$

This function is locally positive-definite about $(p_F, \tilde{R}_{11}) = (0, 1)$ within region Ω_c defined in Eq. (18). Moreover, note that $\|e_{\tilde{R}}\|^2 = \Psi(\tilde{R})(1 - \Psi(\tilde{R}))$ and, then, the bound in Eq. (B2) implies that, inside set Ω_c , the Lyapunov function V_{pf} can be bounded as

$$\|e_{\tilde{R}}\|^2 + \frac{1}{c_1^2} \|p_F\|^2 \leq V_{pf} \leq \frac{1}{1 - c^2} \|e_{\tilde{R}}\|^2 + \frac{1}{c_1^2} \|p_F\|^2 \quad (\text{B3})$$

From Eqs. (1) and (5), the time derivative of V_{pf} along the trajectories of the system is given by

$$\begin{aligned} \dot{V}_{pf} &= e_{\tilde{R}} \cdot \left(\begin{bmatrix} q \\ r \end{bmatrix} - \Pi_R \tilde{R}^T (R_F^D \{\omega_{F/I}\}_F + \{\omega_{D/F}\}_D) \right) \\ &\quad + \frac{2}{c_1^2} p_F \cdot (-\dot{\ell} \mathbf{t} - \omega_{F/I} \times p_F + v \mathbf{w}_1) \end{aligned}$$

The rate commands of Eq. (13), together with the law of Eq. (12) for the rate of progression of the virtual target along the path, lead to

$$\begin{aligned} \dot{V}_{pf} &= -2K_{\tilde{R}} e_{\tilde{R}} \cdot e_{\tilde{R}} + \frac{2}{c_1^2} (-K_\ell (p_F \cdot \mathbf{t})^2 - p_F \cdot (\omega_{F/I} \times p_F) \\ &\quad + vp_F \cdot (\mathbf{w}_1 - (\mathbf{w}_1 \cdot \mathbf{t}) \mathbf{t})) \\ &= -2K_{\tilde{R}} e_{\tilde{R}} \cdot e_{\tilde{R}} - \frac{2K_\ell}{c_1^2} x_F^2 + \frac{2v}{c_1^2} (p_F \cdot (\mathbf{w}_1 - (\mathbf{w}_1 \cdot \mathbf{t}) \mathbf{t})) \end{aligned}$$

Let $p_X(t) \triangleq y_F(t)\mathbf{n}_1(t) + z_F(t)\mathbf{n}_2(t)$ denote the cross-track error, and note that, within set Ω_c , the following bounds hold:

$$\begin{aligned} 0 &< 1 - 2c^2 \leq 1 - 2\Psi(\tilde{R}) = (\mathbf{w}_1 \cdot \mathbf{b}_{1D}) \leq 1, \\ \|p_X\| &\leq \|p_F\| \leq cc_1 \end{aligned}$$

From these bounds, together with the assumption on the UAV speed in Eq. (14), it can be proven that

$$\begin{aligned} \dot{V}_{pf} &\leq -2K_{\tilde{R}} \|e_{\tilde{R}}\|^2 - \frac{2K_\ell}{c_1^2} x_F^2 - \frac{2v_{\min}}{c_1^2(d^2 + c^2 c_1^2)^{\frac{1}{2}}} \|p_X\|^2 \\ &\quad + \frac{2v_{\max}}{c_1^2(1 - 2c^2)} \|p_X\| \|\mathbf{w}_1 \times (\mathbf{w}_1 \times \mathbf{b}_{1D})\| \end{aligned}$$

Then, noting that $\|\mathbf{w}_1 \times (\mathbf{w}_1 \times \mathbf{b}_{1D})\| = 2\|e_{\tilde{R}}\|$, it follows that

$$\begin{aligned} \dot{V}_{pf} &\leq -2K_{\tilde{R}} \|e_{\tilde{R}}\|^2 - \frac{2K_\ell}{c_1^2} x_F^2 - \frac{2v_{\min}}{c_1^2(d^2 + c^2 c_1^2)^{\frac{1}{2}}} \|p_X\|^2 \\ &\quad + \frac{4v_{\max}}{c_1^2(1 - 2c^2)} \|p_X\| \|e_{\tilde{R}}\| \end{aligned}$$

Letting $K_p \triangleq \min \left\{ K_\ell, \frac{v_{\min}}{(d^2 + c^2 c_1^2)^{\frac{1}{2}}} \right\}$ and noting that $\|p_X\| \leq \|p_F\|$, one finds

$$\dot{V}_{pf} \leq -2K_{\tilde{R}} \|e_{\tilde{R}}\|^2 - \frac{2K_p}{c_1^2} \|p_F\|^2 + \frac{4v_{\max}}{c_1^2(1 - 2c^2)} \|p_F\| \|e_{\tilde{R}}\|$$

From the choice for the characteristic distance d and the path-following control parameters K_ℓ and $K_{\tilde{R}}$ in Eq. (15) and the definition of $\bar{\lambda}_{pf}$ in Eq. (17), it follows that

$$\begin{bmatrix} K_{\tilde{R}} & -\frac{v_{\max}}{c_1^2(1 - 2c^2)} \\ -\frac{v_{\max}}{c_1^2(1 - 2c^2)} & \frac{K_p}{c_1^2} \end{bmatrix} \geq \bar{\lambda}_{pf} \begin{bmatrix} \frac{1}{1 - c^2} & 0 \\ 0 & \frac{1}{c_1^2} \end{bmatrix}$$

which implies that, within set Ω_c , the following bound holds:

$$\dot{V}_{pf} \leq -2\bar{\lambda}_{pf} \left(\frac{1}{1 - c^2} \|e_{\tilde{R}}\|^2 + \frac{1}{c_1^2} \|p_F\|^2 \right) \leq -2\bar{\lambda}_{pf} V_{pf}$$

It follows from [57] (Theorem 4.10) that both $\|e_{\tilde{R}}\|$ and $\|p_F\|$ converge exponentially to zero for all the initial conditions inside the compact set Ω_c . \square

Appendix C: Sketch of the Proof of Lemma 2

First, it is shown that the rate commands $q_c(t)$ and $r_c(t)$ are bounded for all $(p_F, e_{\tilde{R}}) \in \Omega_c$. To this end, note that, over the compact set Ω_c , which was introduced in Eq. (18), the following inequalities hold:

$$\|p_F\| \leq cc_1, \quad \Psi(\tilde{R}) \leq c^2$$

These bounds, together with the bound on the UAV speed in Eq. (14) and the assumption on the feasibility of the path, can be used to show that, for all $(p_F, e_{\tilde{R}}) \in \Omega_c$, the rate commands $q_c(t)$ and $r_c(t)$ are bounded. Then, based on the assumption made in Sec. II.C on the

tracking capabilities of the UAV with its autopilot, one has that, for all $(p_F, e_{\tilde{R}}) \in \Omega_c$, the following performance bounds hold:

$$|q_c - q| \leq \gamma_q, \quad |r_c - r| \leq \gamma_r \quad (\text{C1})$$

Next, consider again the Lyapunov function candidate

$$V_{pf}(p_F, \tilde{R}) = \Psi(\tilde{R}) + \frac{1}{c_1^2} \|p_F\|^2$$

From Eqs. (1) and (5), the time derivative of V_{pf} along the trajectories of the system can be expressed as

$$\begin{aligned} \dot{V}_{pf} &= e_{\tilde{R}} \cdot \left(\begin{bmatrix} q_c \\ r_c \end{bmatrix} - \Pi_R \tilde{R}^T (R_F^D \{\omega_{F/I}\}_F + \{\omega_{D/F}\}_D) \right) \\ &\quad + \frac{2}{c_1^2} p_F \cdot (-\dot{\ell}t - \omega_{F/I} \times p_F + v\mathbf{w}_1) - e_{\tilde{R}} \cdot \begin{bmatrix} q_c - q \\ r_c - r \end{bmatrix} \end{aligned}$$

Similar to the proof of Lemma 1, one has that, inside set Ω_c , the following bound holds:

$$\dot{V}_{pf} \leq -2\bar{\lambda}_{pf} \left(\frac{1}{1-c^2} \|e_{\tilde{R}}\|^2 + \frac{1}{c_1^2} \|p_F\|^2 \right) + \|e_{\tilde{R}}\| \left\| \begin{bmatrix} q_c - q \\ r_c - r \end{bmatrix} \right\|$$

where $\bar{\lambda}_{pf}$ was defined in Eq. (17). From the performance bounds in Eq. (C1) and the definition of γ_ω in Eq. (19), it follows that

$$\left\| \begin{bmatrix} q_c - q \\ r_c - r \end{bmatrix} \right\| \leq \gamma_\omega$$

which leads to

$$\dot{V}_{pf} \leq -2\bar{\lambda}_{pf} \left(\frac{1}{1-c^2} \|e_{\tilde{R}}\|^2 + \frac{1}{c_1^2} \|p_F\|^2 \right) + \|e_{\tilde{R}}\| \gamma_\omega$$

The previous inequality can now be rewritten as

$$\begin{aligned} \dot{V}_{pf} &\leq -2\bar{\lambda}_{pf}(1-\delta_\lambda) \left(\frac{1}{1-c^2} \|e_{\tilde{R}}\|^2 + \frac{1}{c_1^2} \|p_F\|^2 \right) \\ &\quad - 2\bar{\lambda}_{pf}\delta_\lambda \left(\frac{1}{1-c^2} \|e_{\tilde{R}}\|^2 + \frac{1}{c_1^2} \|p_F\|^2 \right) + \|e_{\tilde{R}}\| \gamma_\omega \end{aligned}$$

where $0 < \delta_\lambda < 1$. Then, for all $p_F(t)$ and $e_{\tilde{R}}(t)$ satisfying

$$-2\bar{\lambda}_{pf}\delta_\lambda \left(\frac{1}{1-c^2} \|e_{\tilde{R}}\|^2 + \frac{1}{c_1^2} \|p_F\|^2 \right) + \|e_{\tilde{R}}\| \gamma_\omega \leq 0 \quad (\text{C2})$$

one has

$$\begin{aligned} \dot{V}_{pf} &\leq -2\bar{\lambda}_{pf}(1-\delta_\lambda) \left(\frac{1}{1-c^2} \|e_{\tilde{R}}\|^2 + \frac{1}{c_1^2} \|p_F\|^2 \right) \\ &\leq -2\bar{\lambda}_{pf}(1-\delta_\lambda) V_{pf} \end{aligned}$$

The inequality in Eq. (C2) is satisfied outside the bounded set D defined by

$$\begin{aligned} D \triangleq \left\{ (p_F, \tilde{R}) \in \mathbb{R}^3 \times \text{SO}(3) \mid \frac{1}{1-c^2} \left(\|e_{\tilde{R}}\| - \frac{(1-c^2)\gamma_\omega}{4\bar{\lambda}_{pf}\delta_\lambda} \right)^2 \right. \\ \left. + \frac{1}{c_1^2} \|p_F\|^2 < \frac{(1-c^2)\gamma_\omega^2}{16\bar{\lambda}_{pf}^2\delta_\lambda^2} \right\} \end{aligned}$$

One can prove that set D is in the interior of the compact set Ω_b defined by

$$\Omega_b \triangleq \left\{ (p_F, \tilde{R}) \in \mathbb{R}^3 \times \text{SO}(3) \mid \Psi(\tilde{R}) + \frac{1}{c_1^2} \|p_F\|^2 \leq \frac{(1-c^2)\gamma_\omega^2}{4\bar{\lambda}_{pf}^2\delta_\lambda^2} \right\}$$

Then, the design constraint for the performance bounds γ_q and γ_r in Eq. (19) implies that set Ω_b is in the interior of set Ω_c introduced in Eq. (18), that is $\Omega_b \subset \Omega_c$.

With the previous results and using a proof similar to that of Theorem 4.18 in [57], it can be shown that, for every initial state $(p_F(0), \tilde{R}(0)) \in \Omega_c$, there is a time $T_b \geq 0$ such that the following bounds are satisfied:

$$\begin{aligned} V_{pf}(t) &\leq V_{pf}(0) e^{-2\bar{\lambda}_{pf}(1-\delta_\lambda)t}, \quad \forall 0 \leq t < T_b, \\ V_{pf}(t) &\leq \frac{(1-c^2)\gamma_\omega^2}{4\bar{\lambda}_{pf}^2\delta_\lambda^2}, \quad \forall t \geq T_b \end{aligned}$$

The bounds in Eqs. (20) and (21) follow immediately from the previous two bounds and the inequalities in Eq. (B3). \square

Appendix D: Sketch of the Proof of Lemma 3

To prove ISS, it is first shown that the homogeneous equation of the coordination dynamics

$$\dot{\zeta}(t) = F(t)\zeta(t) \quad (\text{D1})$$

is globally uniformly exponentially stable (GUES). To this end, consider the system

$$\dot{\phi}(t) = -a\bar{L}(t)\phi(t) \quad (\text{D2})$$

where a is the proportional coordination control gain introduced in Eq. (26). Letting $D(t)$ be the time-varying incidence matrix, $L(t) = D(t)D^T(t)$, one can rewrite the previous system as $\dot{\phi}(t) = -a(QD(t))(QD(t))^T\phi(t)$. Then, because $QD(t)$ is piecewise constant in time and, in addition, one has that $\|QD(t)\|^2 \leq n$, it can be proven that the system in Eq. (D2) is GUES, and the following bound holds:

$$\|\phi(t)\| \leq k_\lambda \|\phi(0)\| e^{-\gamma_\lambda t}$$

with $k_\lambda = 1$ and $\gamma_\lambda \geq \bar{\gamma}_\lambda \triangleq [an\mu/(1+anT)^2]$. This result can be proven along the same lines as Lemma 5 in [58] or Lemma 3 in [59]. Because $\bar{L}(t)$ is continuous for almost all $t \geq 0$ and uniformly bounded, and the system [Eq. (D2)] is GUES, Lemma 1 in [59] and a similar argument as in [57] (Theorem 4.12) imply that, for any \bar{c}_3 and \bar{c}_4 satisfying $0 < \bar{c}_3 \leq \bar{c}_4$, there exists a continuous, piecewise-differentiable $P_{c_0}(t) = P_{c_0}^T(t)$ such that

$$\bar{c}_1 \mathbb{I}_{n-1} \triangleq \frac{\bar{c}_3}{2an} \mathbb{I}_{n-1} \leq P_{c_0}(t) \leq \frac{\bar{c}_4}{2\bar{\gamma}_\lambda} \mathbb{I}_{n-1} \triangleq \bar{c}_2 \mathbb{I}_{n-1} \quad (\text{D3})$$

$$\dot{P}_{c_0}(t) - a\bar{L}(t)P_{c_0}(t) - aP_{c_0}(t)\bar{L}(t) \leq -\bar{c}_3 \mathbb{I}_{n-1} \quad (\text{D4})$$

Next, define

$$z(t) = S_\zeta \zeta(t) = \begin{bmatrix} \mathbb{I}_{n-1} & 0 \\ -\frac{b}{a} C^T Q^T & \mathbb{I}_{n-1} \end{bmatrix} \zeta(t)$$

and, nothing that $\lambda_{\min}(C^T Q^T Q C)^{-1} = 1$, consider the Lyapunov function candidate

$$V_c(t, z) \triangleq z^T P_c(t) z, \quad P_c(t) \triangleq \begin{bmatrix} P_{c_0}(t) & 0 \\ 0 & \frac{a^3}{b^3} (C^T Q^T Q C)^{-1} \end{bmatrix}$$

The time derivative of V_c along the trajectories of the system is given by

$$\dot{V}_c(t) = z^T(t) \begin{bmatrix} \dot{P}_{c_0}(t) - a\bar{L}(t)P_{c_0}(t) - aP_{c_0}(t)\bar{L}(t) + \frac{b}{a}QCC^TQ^TP_{c_0}(t) + \frac{b}{a}P_{c_0}(t)QCC^TQ^T & P_{c_0}(t)QC - \frac{a}{b}QC \\ C^TQ^TP_{c_0}(t) - \frac{a}{b}C^TQ^T & -2\frac{a^2}{b^2}\mathbb{I}_{n-1} \end{bmatrix} z(t)$$

Now, for any $k_\beta \geq 2$, define $\beta \triangleq k_\beta n$. Then, letting $a > 0$, $\bar{\lambda}_c = \bar{\gamma}_\lambda(1 + \beta)^{-1}$, $b = an\bar{\lambda}_c k_\beta$, and $\bar{c}_3 = \bar{c}_4 = (\bar{\gamma}_\lambda/\bar{\lambda}_c)(2/k_\beta n)$, and noting that $\|QC\| = 1$ and $\lambda_{\max}(C^TQ^TQC)^{-1} = n$, one can use Eqs. (D3) and (D4) and Schur complements to prove that

$$\dot{V}_c(t) \leq -2\bar{\lambda}_c z^T(t) \begin{bmatrix} P_{c_0}(t) & 0 \\ 0 & \frac{a^3}{b^3}(C^TQ^TQC)^{-1} \end{bmatrix} z(t) = -2\bar{\lambda}_c V_c(t)$$

Application of the comparison lemma (see [57], Lemma 3.4]) leads to $V_c(t) \leq V_c(0)e^{-2\bar{\lambda}_c t}$, and because $\min\{\bar{c}_1, \frac{a^3}{b^3}\}\|z(t)\|^2 \leq V_c(t) \leq \max\{\bar{c}_2, \frac{a^3}{b^3}\}\|z(t)\|^2$, one finds that

$$\|\zeta(t)\| \leq \|S_\zeta^{-1}\| \left(\frac{\max\{\bar{c}_2, \frac{a^3}{b^3}n\}}{\min\{\bar{c}_1, \frac{a^3}{b^3}\}} \right)^{\frac{1}{2}} \|\zeta(0)\| e^{-\bar{\lambda}_c t}$$

and consequently the system of Eq. (D1) is GUES. One concludes that the forced system of Eq. (28) is ISS because it is a linear system, the Laplacian $L(t)$ is bounded, the homogeneous equation is GUES, and the speed-tracking error vector $e_v(t)$ is assumed to be bounded for all $t \geq 0$. This implies that the bound in Eq. (29) holds. The constants k_1 and k_2 in Eq. (29) can be derived from a proof similar to those of Theorem 4.19 and Lemma 4.6 in [57].

To prove Eqs. (30) and (31), one can introduce the disagreement vector $\rho(t) \triangleq \Pi\xi(t)$ and use the facts that

$$\xi_i(t) - \xi_j(t) = \rho_i(t) - \rho_j(t), \quad i, j = 1, 2, \dots, n; \quad (\text{D5})$$

$$\|\rho(t)\| = \|\zeta_1(t)\| \quad (\text{D6})$$

$$\zeta_{2,i}(t) = \chi_{I,i}(t) - 1, \quad i = 2, \dots, n \quad (\text{D7})$$

It follows from the relationships of Eqs. (D5) and (D6) that $|\xi_i(t) - \xi_j(t)| \leq 2\|\zeta_1(t)\|$, and thus Eq. (29) leads to Eq. (30) with $k_3 = 2k_2$. On the other hand, from Eqs. (25), (27), and (D7), one obtains

$$\begin{aligned} \dot{\xi}_i(t) - 1 &= -a \sum_{j \in J_1} (\xi_i(t) - \xi_j(t)) + e'_{v,1}(t) \\ \dot{\xi}_i(t) - 1 &= -a \sum_{j \in J_1} (\xi_i(t) - \xi_j(t)) + \zeta_{2,i-1}(t) + e'_{v,i}(t), \\ i &= 2, \dots, n \end{aligned}$$

which, along with the bound in Eq. (29) and the fact that $|e'_{v,i}(t)| \leq [|e_{v,i}(t)|/v_{\min}]$, lead to the bound in Eq. (31) with $k_4 = (2a(n-1) + 1)k_2 + (1/v_{\min})$. \square

Appendix E: Sketch of the Proof of Theorem 1

To simplify the notation in this proof sketch, define the positive constants $v_{c\min}$ and $v_{c\max}$ as $v_{c\min} \triangleq v_{\min} + \gamma_v$ and $v_{c\max} \triangleq v_{\max} - \gamma_v$.

From the assumptions on the initial conditions in Eqs. (37) and (38), along with the choice for the characteristic distance d in Eq. (33), it can be shown that the following bounds hold at time $t = 0$ for all vehicles:

$$v_{c\min} \leq v_{c,j}(0) \leq v_{c\max}, \quad \forall j \in \{1, \dots, n\}$$

With this preliminary result in mind, the claims of the theorem are now proven by contradiction. To this effect, consider one of the UAVs involved in the mission that has not yet reached its final destination, and assume that it violates the results of the theorem, that is either it is

not able to remain inside the prespecified tube centered on its desired path or its speed command goes outside the acceptable feasible range while trying to keep coordination with the other UAVs. Without loss of generality, assume that this UAV is the first one that violates (at least) one of these conditions, and therefore suppose that all other vehicles do satisfy the claims of the theorem. More precisely, consider the i th UAV and suppose that, at time $t > 0$, it has not yet reached the final destination, i.e., $\ell'_i(t) < 1$. Assume that, at this same time instant t , either the path-following errors of the i th UAV are such that $(p_{F,i}(t), \tilde{R}_i(t)) \notin \Omega_c$, or its speed command $v_{c,i}(t)$ does not satisfy the bounds $v_{c\min} \leq v_{c,i}(t) \leq v_{c\max}$ (or both). For all other UAVs, assume that $(p_{F,j}(t), \tilde{R}_j(t)) \in \Omega_c$ and $v_{c\min} \leq v_{c,j}(t) \leq v_{c\max}$, $j \in \{1, \dots, n\}$, $j \neq i$, and for all $\tau \in [0, t]$.

Consider first the case in which $(p_{F,i}(t), \tilde{R}_i(t)) \notin \Omega_c$, while $v_{c\min} \leq v_{c,i}(\tau) \leq v_{c\max}$ for all $\tau \in [0, t]$. For the i th UAV, consider the path-following Lyapunov function candidate $V_{pf,i}(p_{F,i}, \tilde{R}_i) = \Psi(\tilde{R}_i) + (1/c_1^2)\|p_{F,i}\|^2$. Because $(p_{F,i}(0), \tilde{R}_i(0)) \in \Omega_c$ by assumption, and $V_{pf,i}$ evaluated along the system trajectories is continuous and differentiable, one has that, if $(p_{F,i}(t), \tilde{R}_i(t)) \notin \Omega_c$ for some $t > 0$, then there exists a time t' ($0 \leq t' < t$) such that

$$V_{pf,i}(t') = c^2 \quad (\text{E1})$$

$$\dot{V}_{pf,i}(t') > 0 \quad (\text{E2})$$

while

$$V_{pf,i}(\tau) \leq c^2, \quad \forall \tau \in [0, t') \quad (\text{E3})$$

Equations (E1, E3) imply that $\|p_{F,i}(\tau)\| \leq cc_1$ and $\Psi(\tilde{R}_i(\tau)) \leq c^2$ for all $\tau \in [0, t']$. These two bounds, along with the choice for the characteristic distance d in Eq. (33) and the assumption on the UAV dynamics in Eq. (11), imply that $\mathbf{w}_{1,i}(\tau) \cdot \mathbf{t}_i(\tau) \geq c_2 > 0$ and $v_{\min} \leq v_i(\tau) \leq v_{\max}$ for all $\tau \in [0, t']$. A proof similar to the one of Lemma 2 can now be used to show that, for all $\tau \in [0, t']$, $\dot{V}_{pf,i} < 0$ on the boundary of Ω_c , which contradicts the claim in Eqs. (E1) and (E2).

Next, consider the case in which the bounds $v_{c\min} \leq v_{c,i}(t) \leq v_{c\max}$ do not hold, while $(p_{F,i}(t), \tilde{R}_i(t)) \in \Omega_c$ for all $t \in [0, t]$. Let t' ($0 < t' \leq t$) be the first time at which $v_{c\min} \leq v_{c,i} \leq v_{c\max}$ is not satisfied. Then, one has that, at time t' , one of the following bounds holds:

$$v_{c\min} > v_{c,i}(t'), \quad \text{or} \quad v_{c,i}(t') > v_{c\max} \quad (\text{E4})$$

while

$$v_{c\min} \leq v_{c,i}(\tau) \leq v_{c\max}, \quad \forall \tau \in [0, t') \quad (\text{E5})$$

Because $(p_{F,i}(\tau), \tilde{R}_i(\tau)) \in \Omega_c$ for all $\tau \in [0, t']$ by hypothesis, it follows that $\|p_{F,i}(\tau)\| \leq cc_1$ and $\Psi(\tilde{R}_i(\tau)) \leq c^2$ for all $\tau \in [0, t']$. These bounds, along with the choice for the characteristic distance d in Eq. (33), the assumption on the UAV dynamics in Eq. (11), and the bound in Eq. (E5), imply that $\mathbf{w}_{1,i}(\tau) \cdot \mathbf{t}_i(\tau) \geq c_2$ for all $\tau \in [0, t']$ and that $|e_{v,i}(\tau)| \leq \gamma_v$ and $v_{\min} \leq v_i(\tau) \leq v_{\max}$ for all $\tau \in [0, t']$. From this last bound, the continuity of v_i , and the fact that (by hypothesis) the bounds $v_{c\min} \leq v_{c,j}(\tau) \leq v_{c\max}$ hold for all $j \in \{1, \dots, n\}$, $j \neq i$, and for all $\tau \in [0, t']$, it follows that $|e_{v,j}(\tau)| \leq \gamma_v$ and $v_{\min} \leq v_j(\tau) \leq v_{\max}$ for all $j \in \{1, \dots, n\}$, $j \neq i$, and for all $\tau \in [0, t']$. These bounds, along with the hypothesis that $(p_{F,j}(\tau), \tilde{R}_j(\tau)) \in \Omega_c$ for all $j \in \{1, \dots, n\}$, $j \neq i$, and for all $\tau \in [0, t']$, can be used to prove that $e_{v,i}(t')$ is bounded. Then, because the speed-tracking error vector $e_{v,i}(\tau)$ is bounded for all $\tau \in [0, t']$, a proof similar to the one of Lemma 3 can be used to show that the choice of the coordination

control gains a and b in Eq. (34) ensures that there exists a positive constant λ_c such that

$$\|\zeta(\tau)\| \leq k_1 \|\zeta(0)\| e^{-\lambda_c \tau} + k_2 \sup_{s \in [0, \tau]} \|e_v(s)\|, \quad \forall \tau \in [0, t']$$

Because $\|e_v(\tau)\| \leq \sqrt{n}\gamma_v$ for all $\tau \in [0, t']$, it follows that $\|\zeta(t')\| \leq k_1 \|\zeta(0)\| + k_2 \sqrt{n}\gamma_v$. This bound, along with Eqs. (D5) and (D6) and the assumption on the initial condition in Eq. (38), can be used to show that $v_{\min} + \gamma_v \leq v_{c,i}(t') \leq v_{\max} - \gamma_v$, which contradicts the claim in Eq. (E4).

Finally, similar arguments can be used to prove the impossibility of both $(p_{F,i}, \tilde{R}_i) \in \Omega_c$ and $v_{c,\min} \leq v_{c,i} \leq v_{c,\max}$ failing to hold at the exact same time.

Therefore, one has that, for all $i \in \{1, \dots, n\}$ and for all $t \geq 0$, the path-following errors $p_{F,i}(t)$ and $\tilde{R}_i(t)$ satisfy $(p_{F,i}(t), \tilde{R}_i(t)) \in \Omega_c$, while the speed command $v_{c,i}(t)$ verifies the bounds $v_{c,\min} \leq v_{c,i}(t) \leq v_{c,\max}$. From these bounds and the assumption on the UAV dynamics in Eq. (11), it follows that $v_{\min} \leq v_i(\tau) \leq v_{\max}$ for all $i \in \{1, \dots, n\}$ and for all $t \geq 0$. Moreover, the choice for the characteristic distance d in Eq. (33) implies that $\mathbf{w}_{1,i}(\tau) \cdot \mathbf{t}_i(\tau) \geq c_2 > 0$ for all $i \in \{1, \dots, n\}$ and for all $t \geq 0$. Then, the bounds in Eqs. (39)–(41) follow respectively from proofs similar to those of Lemmas 2 and 3. \square

Acknowledgments

This research is supported in part by United States Special Operations Command, Office of Naval Research, Air Force Office of Scientific Research, Army Research Office, European Commission FP7 MORPH Project, and Fundação para a Ciência e a Tecnologia.

References

- [1] Kaminer, I., Pascoal, A. M., Hallberg, E., and Silvestre, C., "Trajectory Tracking for Autonomous Vehicles: An Integrated Approach to Guidance and Control," *Journal of Guidance, Control, and Dynamics*, Vol. 21, No. 1, 1998, pp. 29–38.
doi:10.2514/2.4229
- [2] Kim, Y., and Mesbahi, M., "On Maximizing the Second Smallest Eigenvalue of State-Dependent Graph Laplacian," *IEEE Transactions on Automatic Control*, Vol. 51, No. 1, 2006, pp. 116–120.
doi:10.1109/TAC.2005.861710
- [3] Tsitsiklis, J. N., and Athans, M., "Convergence and Asymptotic Agreement in Distributed Decision Problems," *IEEE Transactions on Automatic Control*, Vol. 29, No. 1, 1984, pp. 42–50.
doi:10.1109/TAC.1984.1103385
- [4] Sepulchre, R., Paley, D., and Leonard, N., *Collective Motion and Oscillator Synchronization*, Vol. 309, Lecture Notes in Control and Information Sciences, Springer–Verlag, Berlin, 2005, pp. 189–206.
- [5] Jadbabaie, A., Lin, J., and Morse, A. S., "Coordination of Groups of Mobile Autonomous Agents Using Nearest Neighbor Rules," *IEEE Transactions on Automatic Control*, Vol. 48, No. 6, 2003, pp. 988–1001.
doi:10.1109/TAC.2003.812781
- [6] Lin, Z., Francis, B. A., and Maggiore, M., "State Agreement for Continuous-Time Coupled Nonlinear Systems," *SIAM Journal on Control and Optimization*, Vol. 46, No. 1, 2007, pp. 288–307.
doi:10.1137/050626405
- [7] Egerstedt, M., and Hu, X., "Formation Constrained Multi-Agent Control," *IEEE Transactions on Robotics and Automation*, Vol. 17, No. 6, Dec. 2001, pp. 947–951.
doi:10.1109/70.976029
- [8] Saber, R. O., Dunbar, W. B., and Murray, R. M., "Cooperative Control of Multi-Vehicle Systems Using Cost Graphs and Optimization," *Proceedings of the American Control Conference*, Denver, CO, IEEE, Piscataway, NJ, June 2003, pp. 2217–2222.
- [9] Fax, J. A., and Murray, R. M., "Information Flow and Cooperative Control of Vehicle Formations," *IEEE Transactions on Automatic Control*, Vol. 49, No. 9, 2004, pp. 1465–1476.
doi:10.1109/TAC.2004.834433
- [10] Dunbar, W. B., and Murray, R. M., "Distributed Receding Horizon Control for Multi-Vehicle Formation Stabilization," *Automatica*, Vol. 42, No. 4, 2006, pp. 549–558.
doi:10.1016/j.automatica.2005.12.008
- [11] Ghabcheloo, R., Pascoal, A. M., Silvestre, C., and Kaminer, I., "Coordinated Path Following Control of Multiple Wheeled Robots Using Linearization Techniques," *International Journal of Systems Science*, Vol. 37, No. 6, 2006, pp. 399–414.
doi:10.1080/00207720500438324
- [12] Stevenson, D., Wheeler, M., Campbell, M. E., Whitacre, W. W., Rysdyk, R. T., and Wise, R., "Cooperative Tracking Flight Test," *AIAA Guidance, Navigation, and Control Conference*, AIAA, Aug. 2007; also Paper 2007-6756.
- [13] Keviczky, T., Borrelli, F., Fregene, K., Godbole, D., and Balas, G. J., "Decentralized Receding Horizon Control and Coordination of Autonomous Vehicle Formations," *IEEE Transactions on Control System Technology*, Vol. 16, No. 1, Jan. 2008, pp. 19–33.
doi:10.1109/TCST.2007.903066
- [14] Schouwenaars, T., How, J., and Feron, E., "Decentralized Cooperative Trajectory Planning of Multiple Aircraft with Hard Safety Guarantees," *AIAA Guidance, Navigation, and Control Conference*, AIAA, Aug. 2004; also Paper 2004-5141.
- [15] McLain, T. W., and Beard, R. W., "Coordination Variables, Coordination Functions, and Cooperative Timing Missions," *Journal of Guidance, Control, and Dynamics*, Vol. 28, No. 1, 2005, pp. 150–161.
doi:10.2514/1.5791
- [16] Ousingsawat, J., and Campbell, M. E., "Optimal Cooperative Reconnaissance Using Multiple Vehicles," *Journal of Guidance, Control, and Dynamics*, Vol. 30, No. 1, 2007, pp. 122–132.
doi:10.2514/1.19147
- [17] Scholte, E., and Campbell, M. E., "Robust Nonlinear Model Predictive Control with Partial State Information," *IEEE Transactions on Control System Technology*, Vol. 16, No. 4, July 2008, pp. 636–651.
doi:10.1109/TCST.2007.912120
- [18] Kuwata, Y., and How, J. P., "Cooperative Distributed Robust Trajectory Optimization Using Receding Horizon MILP," *IEEE Transactions on Control System Technology*, Vol. 19, No. 2, March 2011, pp. 423–431.
doi:10.1109/TCST.2010.2045501
- [19] Fang, L., Antsaklis, P. J., and Tzimas, A., "Asynchronous Consensus Protocols: Preliminary Results, Simulations and Open Questions," *Proceedings of the IEEE Conference on Decision and Control*, Seville, Spain, IEEE, Piscataway, NJ, Dec. 2005, pp. 2194–2199.
- [20] Mesbahi, M., "On State-Dependent Dynamic Graphs and Their Controllability Properties," *IEEE Transactions on Automatic Control*, Vol. 50, No. 3, 2005, pp. 387–392.
doi:10.1109/TAC.2005.843858
- [21] Stilwell, D. J., and Bishop, B. E., "Platoons of Underwater Vehicles," *IEEE Control Systems Magazine*, Vol. 20, No. 6, Dec. 2000, pp. 45–52.
doi:10.1109/37.887448
- [22] Stilwell, D. J., Boltt, E. M., and Roberson, D. G., "Sufficient Conditions for Fast Switching Synchronization in Time-Varying Network Topologies," *SIAM Journal of Applied Dynamical Systems*, Vol. 5, No. 1, 2006, pp. 140–156.
doi:10.1137/050625229
- [23] Cao, M., Spielman, D. A., and Morse, A. S., "A Lower Bound on Convergence of a Distributed Network Consensus Algorithm," *Proceedings of the IEEE Conference on Decision and Control*, Seville, Spain, Dec. 2005, pp. 2356–2361.
- [24] Mesbahi, M., and Hadaegh, F. Y., "Formation Flying Control of Multiple Spacecraft via Graphs, Matrix Inequalities, and Switching," *Journal of Guidance, Control, and Dynamics*, Vol. 24, No. 2, 2001, pp. 369–377.
doi:10.2514/2.4721
- [25] Song, Y. D., Li, Y., and Liao, X. H., "Orthogonal Transformation Based Robust Adaptive Close Formation Control of Multi-UAVs," *Proceedings of the American Control Conference*, Vol. 5, Portland, OR, IEEE, Piscataway, NJ, June 2005, pp. 2983–2988.
- [26] Stipanović, D. M., İnalhan, G., Teo, R., and Tomlin, C. J., "Decentralized Overlapping Control of a Formation of Unmanned Aerial Vehicles," *Automatica*, Vol. 40, No. 8, 2004, pp. 1285–1296.
doi:10.1016/j.automatica.2004.02.017
- [27] Skjetne, R., Moi, S., and Fossen, T. I., "Nonlinear Formation Control of Marine Craft," *Proceedings of the IEEE Conference on Decision and Control*, Vol. 2, Las Vegas, NV, IEEE, Piscataway, NJ, Dec. 2002, pp. 1699–1704.
- [28] Fossen, T. I., *Marine Control Systems: Guidance, Navigation and Control of Ships, Rigs and Underwater Vehicles*, Marine Cybernetics, Norway, 2002.
- [29] Pereira, F. L., and de Sousa, J. B., "Coordinated Control of Networked Vehicles: An Autonomous Underwater System," *Automation and Remote Control*, Vol. 65, No. 7, July 2004, pp. 1037–1045.
doi:10.1023/B:AURC.0000038711.03622.09
- [30] Ghabcheloo, R., Aguiar, A. P., Pascoal, A. M., Silvestre, C., Kaminer, I., and Hespanha, J. P., "Coordinated Path-Following Control of Multiple Underactuated Autonomous Vehicles in Presence of Communication Failures," *Proceedings of the IEEE Conference on Decision and*

- Control*, San Diego, CA, IEEE, Piscataway, NJ, Dec. 2006, pp. 4345–4350.
- [31] Ihle, I.-A. F., “Coordinated Control of Marine Craft,” Ph.D. Thesis, Norwegian Univ. of Science and Technology, Trondheim, Norway, Sept. 2006.
- [32] Arrichiello, F., Chiaverini, S., and Fossen, T. I., “Formation Control of Marine Surface Vessels Using the Null-Space-Based Behavioral Control,” *Group Coordination and Cooperative Control*, edited by Pettersen, K. Y., Gravdahl, J. T., and Nijmeijer, H., Vol. 336, Lecture Notes in Control and Information Sciences, Springer-Verlag, Berlin, 2006, pp. 1–19.
- [33] Breivik, M., Subbotin, M. V., and Fossen, T. I., “Kinematic Aspects of Guided Formation Control in 2D,” *Group Coordination and Cooperative Control*, edited by Pettersen, K. Y., Gravdahl, J. T., and Nijmeijer, H., Vol. 336, Lecture Notes in Control and Information Sciences, Springer-Verlag, Berlin, 2006, pp. 55–74.
- [34] Ihle, I.-A. F., Jouffroy, J., and Fossen, T. I., “Robust Formation Control of Marine Craft Using Lagrange Multipliers,” *Group Coordination and Cooperative Control*, edited by Pettersen, K. Y., Gravdahl, J. T., and Nijmeijer, H., Vol. 336, Lecture Notes in Control and Information Sciences, Springer-Verlag, Berlin, 2006, pp. 113–129.
- [35] Kyrkjebø, E., “Motion Coordination of Mechanical Systems: Leader-Follower Synchronization of Euler-Lagrange Systems Using Output Feedback Control,” Ph.D. Thesis, Norwegian Univ. of Science and Technology, Trondheim, Norway, April 2007.
- [36] Breivik, M., Hovstein, V. E., and Fossen, T. I., “Ship Formation Control: A Guided Leader-Follower Approach,” *Proceedings of the IFAC World Congress*, Seoul, South Korea, Elsevier, Oxford, England, U.K., July 2008.
- [37] Aguiar, A. P., Hespanha, J. P., and Kokotović, P. V., “Performance Limitations in Reference Tracking and Path Following for Nonlinear Systems,” *Automatica*, Vol. 44, No. 3, 2008, pp. 598–610. doi:10.1016/j.automatica.2007.06.030
- [38] Kaminer, I., Yakimenko, O. A., Dobrokhodov, V., Pascoal, A. M., Hovakimyan, N., Patel, V. V., Cao, C., and Young, A. Y., “Coordinated Path Following for Time-Critical Missions of Multiple UAVs via \mathcal{L}_1 Adaptive Output Feedback Controllers,” *AIAA Guidance, Navigation, and Control Conference*, AIAA, Aug. 2007; also Paper 2007-6409.
- [39] Aguiar, A. P., and Pascoal, A. M., “Coordinated Path-Following Control for Nonlinear Systems with Logic-Based Communication,” *Proceedings of the IEEE Conference on Decision and Control*, New Orleans, LA, IEEE, Piscataway, NJ, Dec. 2007, pp. 1473–1479.
- [40] Aguiar, A. P., Kaminer, I., Ghabcheloo, R., Pascoal, A. M., Xargay, E., Hovakimyan, N., Cao, C., and Dobrokhodov, V., “Time-Coordinated Path Following of Multiple UAVs over Time-Varying Networks Using \mathcal{L}_1 Adaptation,” *AIAA Guidance, Navigation, and Control Conference*, AIAA, Aug. 2008; also Paper 2008-7131.
- [41] Ghabcheloo, R., Kaminer, I., Aguiar, A. P., and Pascoal, A. M., “A General Framework for Multiple Vehicle Time-Coordinated Path Following Control,” *Proceedings of the American Control Conference*, St. Louis, MO, IEEE, Piscataway, NJ, June 2009, pp. 3071–3076.
- [42] Ghabcheloo, R., Aguiar, A. P., Pascoal, A. M., Silvestre, C., Kaminer, I., and Hespanha, J. P., “Coordinated Path-Following in the Presence of Communication Losses and Delays,” *SIAM Journal on Control and Optimization*, Vol. 48, No. 1, 2009, pp. 234–265. doi:10.1137/060678993
- [43] Kaminer, I., Pascoal, A. M., Xargay, E., Hovakimyan, N., Cao, C., and Dobrokhodov, V., “Path Following for Unmanned Aerial Vehicles Using \mathcal{L}_1 Adaptive Augmentation of Commercial Autopilots,” *Journal of Guidance, Control, and Dynamics*, Vol. 33, No. 2, 2010, pp. 550–564. doi:10.2514/1.42056
- [44] Xargay, E., Dobrokhodov, V., Kaminer, I., Pascoal, A. M., Hovakimyan, N., and Cao, C., “Time-Critical Cooperative Control for Multiple Autonomous Systems,” *IEEE Control Systems Magazine*, Vol. 32, No. 5, Oct. 2012, pp. 49–73. doi:10.1109/MCS.2012.2205477
- [45] Micaelli, A., and Samson, C., “Trajectory Tracking for Unicycle-Type and Two-Steering-Wheels Mobile Robot,” National Institute for Research in Computer Science and Control TR-2097, Sophia-Antipolis, France, Nov. 1993.
- [46] Soetanto, D., Lapierre, L., and Pascoal, A. M., “Adaptive, Non-Singular Path-Following Control of Dynamic Wheeled Robots,” *Proceedings of the International Conference on Advanced Robotics*, Coimbra, Portugal, IEEE, Piscataway, NJ, June–July 2003, pp. 1387–1392.
- [47] Bishop, R. L., “There Is More Than One Way to Frame a Curve,” *American Mathematical Monthly*, Vol. 82, No. 3, 1975, pp. 246–251. doi:10.2307/2319846
- [48] Hanson, A. J., and Ma, H., “Parallel Transport Approach to Curve Framing,” Indiana Univ. Computer Science Department TR TR425, 1995.
- [49] Olfati-Saber, R., Fax, J. A., and Murray, R. M., “Consensus and Cooperation in Networked Multi-Agent Systems,” *Proceedings of the IEEE*, Vol. 95, No. 1, 2007, pp. 215–233. doi:10.1109/JPROC.2006.887293
- [50] Biggs, N., *Algebraic Graph Theory*, Cambridge Univ. Press, New York, 1993.
- [51] Arcak, M., “Passivity as a Design Tool for Group Coordination,” *IEEE Transactions on Automatic Control*, Vol. 52, No. 8, 2007, pp. 1380–1390. doi:10.1109/TAC.2007.902733
- [52] Lee, T., Leok, M., and McClamroch, N. H., “Control of Complex Maneuvers for a Quadrotor UAV Using Geometric Methods on $SE(3)$,” *IEEE Transactions on Automatic Control* (submitted for publication).
- [53] Cicchella, V., Xargay, E., Dobrokhodov, V., Kaminer, I., Pascoal, A. M., and Hovakimyan, N., “Geometric 3D Path-Following Control for a Fixed-Wing UAV on $SO(3)$,” *AIAA Guidance, Navigation, and Control Conference*, AIAA, Aug. 2011; also Paper 2011-6415.
- [54] Xargay, E., Choe, R., Hovakimyan, N. H., and Kaminer, I., “Convergence of a PI Coordination Protocol in Networks with Switching Topology and Quantized Measurements,” *Proceedings of the IEEE Conference on Decision and Control*, Maui, HI, IEEE, Piscataway, NJ, Dec. 2012, pp. 1387–1392.
- [55] Clement, M. R., Bourakov, E., Jones, K. D., and Dobrokhodov, V., “Exploring Network-Centric Information Architectures for Unmanned Systems Control and Data Dissemination,” *AIAA Infotech@Aerospace*, AIAA, April 2009; also Paper 2009-1999.
- [56] Flynn, M. T., Jürgens, R., and Cantrell, T. L., “Employing ISR: SOF Best Practices,” *Joint Force Quarterly*, Vol. 50, July 2008, pp. 56–61.
- [57] Khalil, H. K., *Nonlinear Systems*, 3rd ed., Prentice-Hall, Englewood Cliffs, NJ, 2002.
- [58] Lora, A., and Panteley, E., “Uniform Exponential Stability of Linear Time-Varying Systems: Revisited,” *Systems & Control Letters*, Vol. 47, No. 1, Sept. 2002, pp. 13–24. doi:10.1016/S0167-6911(02)00165-2
- [59] Panteley, E., and Lora, A., “Uniform Exponential Stability for Families of Linear Time-Varying Systems,” *Proceedings of the IEEE Conference on Decision and Control*, Sydney, Australia, IEEE, Piscataway, NJ, Dec. 2000, pp. 1948–1953.